MYXOMA VIRUS THERAPY FOR NEUROBLASTOMA

By

NIKEA C. AYTES

A THESIS PRESENTED TO THE GRADUATE SCHOOL
OF THE UNIVERSITY OF FLORIDA IN PARTIAL FULFILLMENT
OF THE REQUIREMENTS FOR THE DEGREE OF
MASTER OF SCIENCE

UNIVERSITY OF FLORIDA

2013

This work is dedicated to the glory of my heart and my salvation, Jesus Christ.

ACKNOWLEDGMENTS

I would like to thank Grant McFadden for his mentorship and commitment to my professional development. I must thank all of the past and present members of the McFadden lab who have taken the time to invest in my training. Of my fellow lab members, I am especially appreciative of Winnie Chan. Thank you for your assistance with much of the *in vivo* and flow cytometry work, including those times that interrupted the holiday or weekend. I must also say thank you to Dot Smith for her professional support and sincere encouragement.

I am in debt to all of the faculty and staff of the University of Florida College of Medicine, including Rich Condit for his relentless support. In addition, I thank my supervisory committee for the value added to my project. I thank Kris Minkoff for her help in navigating the nuances of a program maintained under two different colleges. As part of the seed cohort for the Translational Biotechnology program, I would like to recognize Richard Snyder for birthing this opportunity, as well as Tammy Mandell for her gentle guidance. I recognize that much of the perspective and skills I have acquired would not have happened without my fellow classmates, and so I thank you also.

Finally, I express my gratitude for the strength and leadership of my loving parents, the heartwarming support of my younger brothers, and the forever encouragement of my most steadfast companion, Jerrell.

This work supported by the NSF Master of Science Program in Translational Biotechnology at the University of Florida.

TABLE OF CONTENTS

page

LIST OF TABLES

LIST OF FIGURES

Abstract of Thesis Presented to the Graduate School
of the University of Florida in Partial Fulfillment of the
Requirements for the Degree of Master of Science

MYXOMA VIRUS THERAPY FOR NEUROBLASTOMA

By

Nikea C. Aytes

August 2013

Chair: Grant McFadden
Major: Medical Sciences – Translational Biotechnology

The most widespread childhood cancer located outside of the brain is neuroblastoma (NB). It accounts for 12% of all childhood cancer-related deaths and affects 10.5 million children annually, usually in infants younger than five. Toxic rounds of surgery, chemotherapy, and radiation still fail to provide relapse-free survival in high-risk children. In addition to tumor reduction, the more severe methods obliterate the child's protective immune system. Patient's hematopoietic stem cells (harvested from the bone marrow or cytokine-mobilized blood) is therefore collected before treatment and saved to allow for later re-engraftment of immune stem cells. One continuing concern is that the autologous transplant samples harbor contaminating NB cells.

We are currently testing oncolytic virotherapy as a self-replicating and easily administered tool to remove any residual cancer cells from the auto-transplant sample. Myxoma Virus (MYXV) has already been proven naturally selective for the purging of other classes of cancer cells from bone marrow samples. MYXV also lacks the ability to productively infect normal primary $CD34^+$ hematopoietic stem cells. The current study shows that MYXV can infect and kill the human neuroblastoma cell line, SK-N-AS, *in vitro*. In addition, when cells are treated with MYXV prior to tail vein injection into NSG

mice, we observe a decrease in tumor engraftment *in vivo*, and this is accompanied by reduced disease phenotypes. Results from this study also provide insight to suggestions for increasing MYXV treatment efficiency. We have established a xenograft model to test for the *ex vivo* purging of contaminating neuroblastoma cells from transplant samples. We support the continued investigation of MYXV as a potential therapeutic strategy for the treatment of the pediatric disease neuroblastoma.

CHAPTER 1
INTRODUCTION

Myxoma Virus Therapy

The rabbit poxvirus, Myxoma Virus (MYXV), is being developed as a therapeutic option for different classes of human cancer[1, 2, 3]. A member of the Poxviridae family, MYXV is composed of a large double-stranded DNA genome that lends itself as relatively amenable for genetic manipulation. While most DNA viruses will enter and replicate within the nucleus of host cells, MYXV and all other poxviruses exhibit the unique feature of maintaining a complete life cycle that is restricted to the cytoplasm[4]. This means that concerns over viral integration into the host genome are non-existent for MYXV therapy.

The complete replication cycle of MYXV is presented in Figure 1-1. This shows the binding of individual virions to cell surfaces, fusion/entry, and release into the cytoplasm, followed by the temporally regulated events of DNA synthesis, transcription, and protein synthesis, all under direction of the virus[5]. Figure 1-1 shows how virus replication will proceed within permissive cells, and so this is how MYXV replication would progress within cancer cells that are susceptible to this virotherapy.

Outside a subset of lagomorphs (the European rabbit), MYXV is not associated with pathogenic disease and the virus does not replicate in any other species (including humans or mice) [4]. One exception to this strict host tropism is in the case of many human cancer cells[6]. Most cancer cells no longer maintain the full array of intact innate immune defenses, which prevent MYXV replication in normal, healthy primary cells. This means that MYXV is able to distinguish between the intracellular environments of cancerous versus non-cancerous cells (based on the ability to complete its replication

cycle, or not). We know that many human cancer cells, for example, experience dysregulated interferon and tumor necrosis factor signaling, which allows for productive MYXV infection[7, 8]. On the other hand, MYXV can bind to many non-cancerous primary human cells under *ex vivo* conditions[9] but the extent of subsequent virus replication varies substantially, depending on the extent of production of inhibitory interferon and/or TNF[7]. Indeed, one of the few primary human cell types that cannot be infected by MYXV is $CD34^+$ hematopoietic stem cells, which do not bind MYXV virions[10, 1]. In all tested non-rabbit hosts, however, MYXV does not replicate to any substantial degree within normal tissues, for example even following systemic administration into highly immunodeficient mice, unless tumor cells are present [4, 11]. The specificity of oncolytic viruses for replication in cancer cells, while excluding non-cancerous cells, is the basis of oncolytic virotherapy; this concept is represented in Figure 1-2[12].

Neuroblastoma

Neuroblastoma is the leading cause of pediatric cancer for solid tumors that occur outside of the brain. It accounts for 12% of all childhood cancer-related deaths[13] and affects 10.5 million children annually[14]. Most of these are 5 years of age or younger. Sixty-five percent of afflicted children develop primary tumors in the adrenal gland, but they may arise anywhere along the sympathetic nervous system and clinical symptoms vary with location[15]. Neuroblastoma is heterogeneous in both biology and clinical behavior, a challenge in the development of appropriate therapies.

Heterogeneous Cause of Disease

For neuroblastoma, a single common genetic cause for disease initiation has not been identified. In a recent study of somatic mutations in high-risk patients, whole-exome, genome, and transcriptome sequencing revealed that there are very few shared

mutations among patients and these occur at low frequencies[16]. Some of these commonalities have nevertheless been implicated as genetic markers of disease and are described in the following. Two known associations with high-risk disease phenotypes include the over-amplification of MYCN and the deletion of the short arm on chromosome 1[15]. Cases of neuroblastoma are not always spontaneous and do not always arise from the germline, as there exists great diversity here as well. It is known that familial cases of neuroblastoma arise from activating mutations in the ALK oncogene[17] or through loss-of-function in PHOX2B[18, 19].

In adult cancers, individuals are more likely to accumulate genetic mutations with increasing age. This leads to the neoplastic growth of otherwise healthy somatic cells. However, neuroblastoma patients maintain a young age at diagnosis (a median of 17 months) [20]. This early onset is characteristic of abnormal embryonic development. Many disease markers of neuroblastoma (ALK, PHOX2B, and MYCN) have been tied to different stages of embryogenesis [21, 22]. In normal sympathetic nervous system (SNS) development, pluripotent neural crest cells arise from the neural tube formed by the ectodermal layer. These neural crest cells are SNS precursors that then migrate through a pathway directed by environmental signals to induce differentiation, cell lineage commitment, and programmed cell death[23, 24]. Disruption in the regulation of these signaling pathways causes aberrant tissue formation. Since the loss of normal cell signaling can occur at any point along the developmental pathway, this is one explanation for the characteristic heterogeneous disease of neuroblastoma[21, 22].

Disease Staging and Standard of Care

Neuroblastoma patients may experience a number of disease phenotypes, ranging from extremes of both high and low risk. Prediction of individual response to

treatment (prognosis) and the “staging” of patients into different risk levels are important for the design of appropriate treatment regimens. Included here are descriptions of the International Neuroblastoma Staging System (INSS) [25], and examples of its modification into risk stratification (Table 1-1[15] and Table 1-2[15]). Overall, staging is used to place children into low, intermediate, and high, risk groups according to various factors and markers of disease[15, 26]. Multimodal therapy for neuroblastoma often includes surgery, chemotherapy, and radiation, along with the more recently developed tissue-specific immunotherapy and differentiation therapy[27]. For neuroblastoma, disease staging is an integral part of treatment planning (Figure 1-3[27]). More than half of all children diagnosed with neuroblastoma are considered high-risk (INSS Stage 4). These patients receive myeloablative chemotherapy followed by autologous hematopoietic stem cell transplant (HSCT) to reconstitute the immune system[28, 29]. Most will experience disease relapse and low survival rates.

Research Outline and Rationale

It has already been shown that neuroblastoma cancer cells can persist within HSC samples of high-risk patients. These HSCs are then later returned to patients following myeloablative therapy, and this may be a source of recurrent disease. The most direct study of neuroblastoma was completed in 1994, utilizing patient bone marrow cells that were harvested and then marked with the neomycin resistance gene. In all three cases of patient relapse, genetic analysis was found to support the persistence of tumor-initiating cells derived from the patient’s autologous HSC graft[30]. Standard of care does not currently include the removal or “purging” of these contaminating cancer cells, though there has been some clinical investigation into the use of $CD34^+$ selection of the needed stem cells as a purging strategy [31, 32]. The innate

ability of MYXV to discriminate between cancerous and non-cancerous cells renders it a unique candidate for use as a biological purging agent. Removal of residual neuroblastoma from patient autografts may reduce the occurrence of relapse and improve long-term survival rates. The objective of this thesis is to study the potential of MYXV to act as a purging agent for neuroblastoma cells that could potentially contaminate autologous stem cell transplant samples. The specific aims are to: 1) demonstrate *in vitro* sensitivity and 2) develop an *in vivo* model of xenotransplantation, 3) to assess MYXV therapy for the human neuroblastoma cell line, SK-N-AS.

Table 1-1. International Neuroblastoma Staging System[15]

INSS Stage	Description
Stage 1	Localized tumor with complete gross excision with or without microscopic residual disease; representative ipsilateral lymph nodes negative for tumor microscopically (nodes attached to and removed with the primary tumor may be positive)
Stage 2A	Localized tumor with incomplete gross resection; representative ipsilateral nonadherent lymph nodes negative for tumor microscopically
Stage 2B	Localized tumor with or without complete gross excision with ipsilateral nonadherent lymph nodes positive for tumor; enlarged contralateral lymph nodes must be negative microscopically
Stage 3	Unresectable unilateral tumor infiltrating across the midline with or without regional lymph node involvement, localized unilateral tumor with contralateral regional lymph node involvement or midline tumor with bilateral extension by infiltration (unresectable) or by lymph node involvement
Stage 4	Any primary tumor with dissemination to distant lymph nodes, bone, bone marrow, liver, skin, or other organs (except 4S)
Stage 4S	Localized primary tumor (as defined for stage 1, 2A or 2B) with dissemination limited to skin, liver, or bone marrow (< 1 yr age)

Table 1-2. Children's Oncology Group neuroblastoma risk stratification[15]

Risk Group	Stage	Age	MYCN status	Ploidy	Shimada index
Low risk	1	Any	Any	Any	Any
Low risk	2a/2b	Any	Not amplified	Any	Any
High risk	2a/2b	Any	Amplified	Any	Any
Intermediate	3	$\geq$ 547 d	Not amplified	Any	Any
Intermediate	3	$\geq$ 547 d	Not amplified	Any	FH
High risk	3	Any	Amplified	Any	Any
High risk	3	$\geq$ 547 d	Not amplified	Any	UH
High risk	4	< 365 d	Amplified	Any	Any
Intermediate	4	< 365 d	Not amplified	Any	Any
High risk	4	365 to < 547 d	Amplified	Any	Any
High risk	4	365 to < 547 d	Any	DI = 1	Any
High risk	4	365 to < 47 d	Any	Any	UH
Intermediate	4	365 to < 547 d	Not amplified	DI > 1	FH
High risk	4	$\geq$ 547 d	Any	Any	Any
Low risk	4s	< 365 d	Not amplified	DI >1	FH
Intermediate	4s	< 365 d	Not amplified	DI = 1	Any
Intermediate	4s	< 365 d	Not amplified	Any	UH
High risk	4s	< 365 d	Amplified	Any	Any

DI: DNA index, FH: favorable histology, UH: unfavorable histology

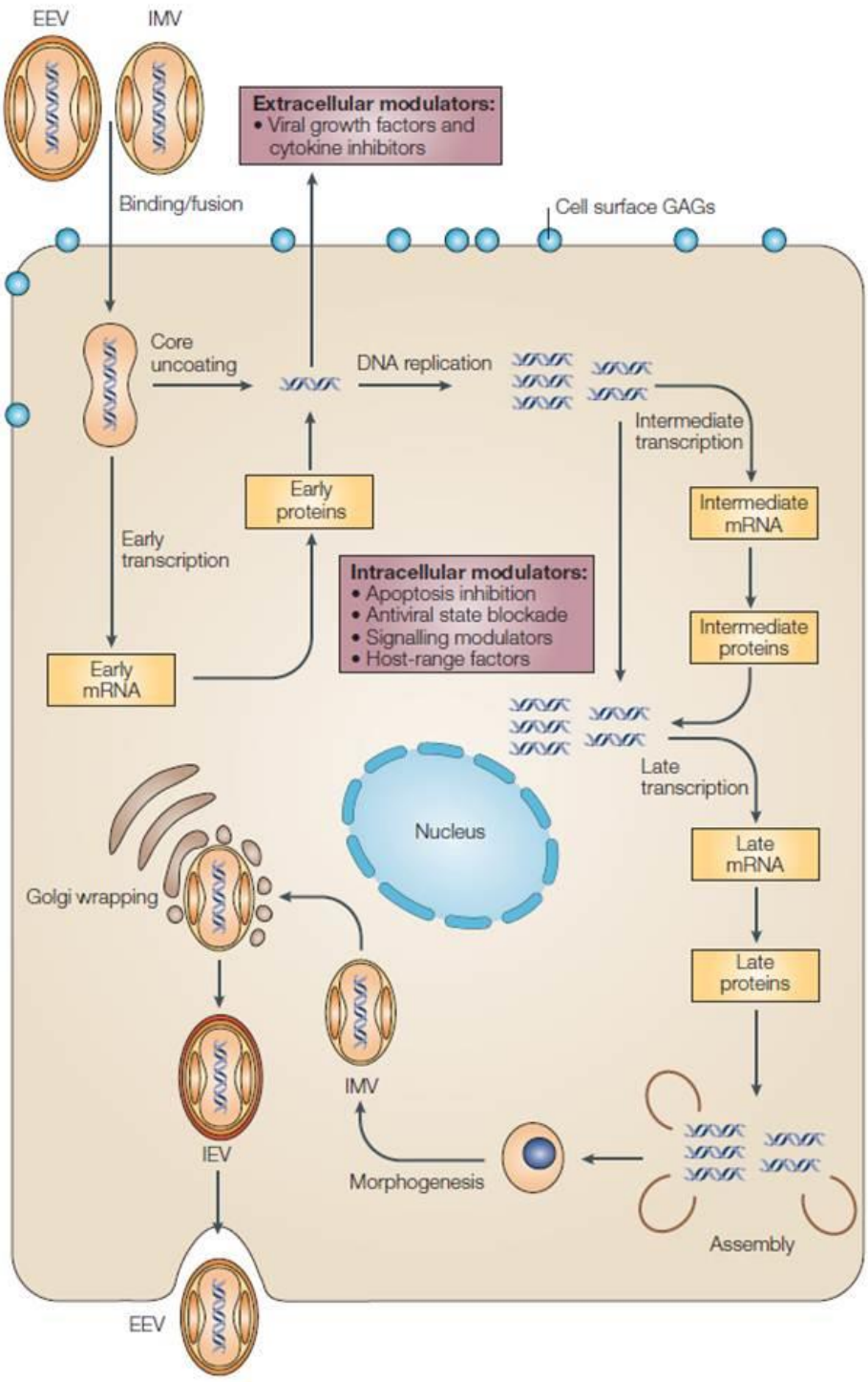

Figure 1-1. Poxvirus replication cycle in permissive cells[5].

Reprinted by permission from [Macmillan Publishers Ltd] (Nature Reviews Microbiology 3, 201-213 | doi:10.1038/nrmicro1099), copyright (2005).

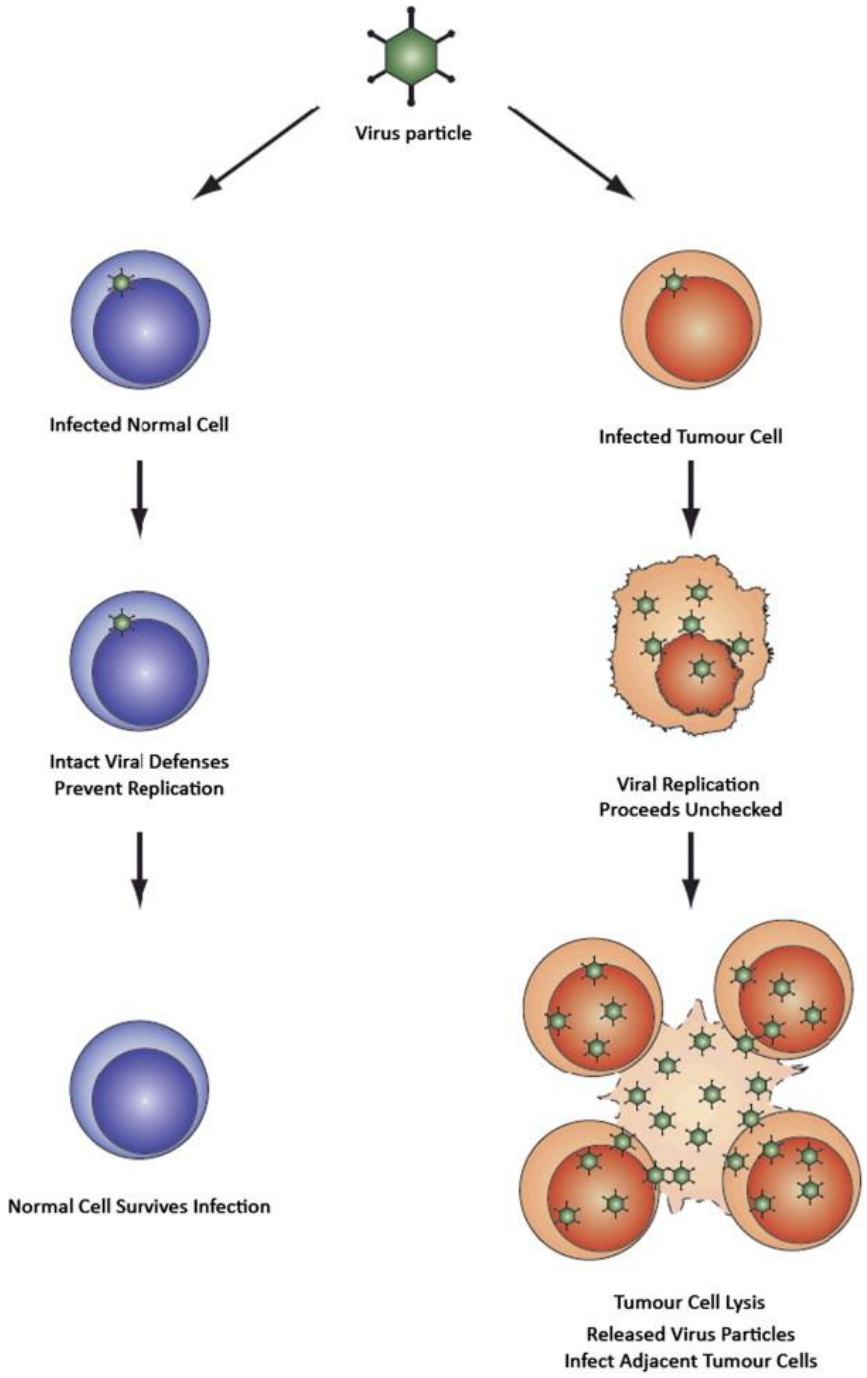

Figure 1-2. The discrimination of cancer cells for oncolytic virotherapy[12].

Reprinted from Cancer Treatment Reviews, 37, Bourke, M. G., S. Salwa, K. J. Harrington, M. J. Kucharczyk, P. F. Forde, M. de Kruijf, D. Soden, M. Tangney, J. K. Collins, and G. C. O'Sullivan, The emerging role of viruses in the treatment of solid tumours, Pages 618-632, Copyright (2010), with permission from Elsevier.

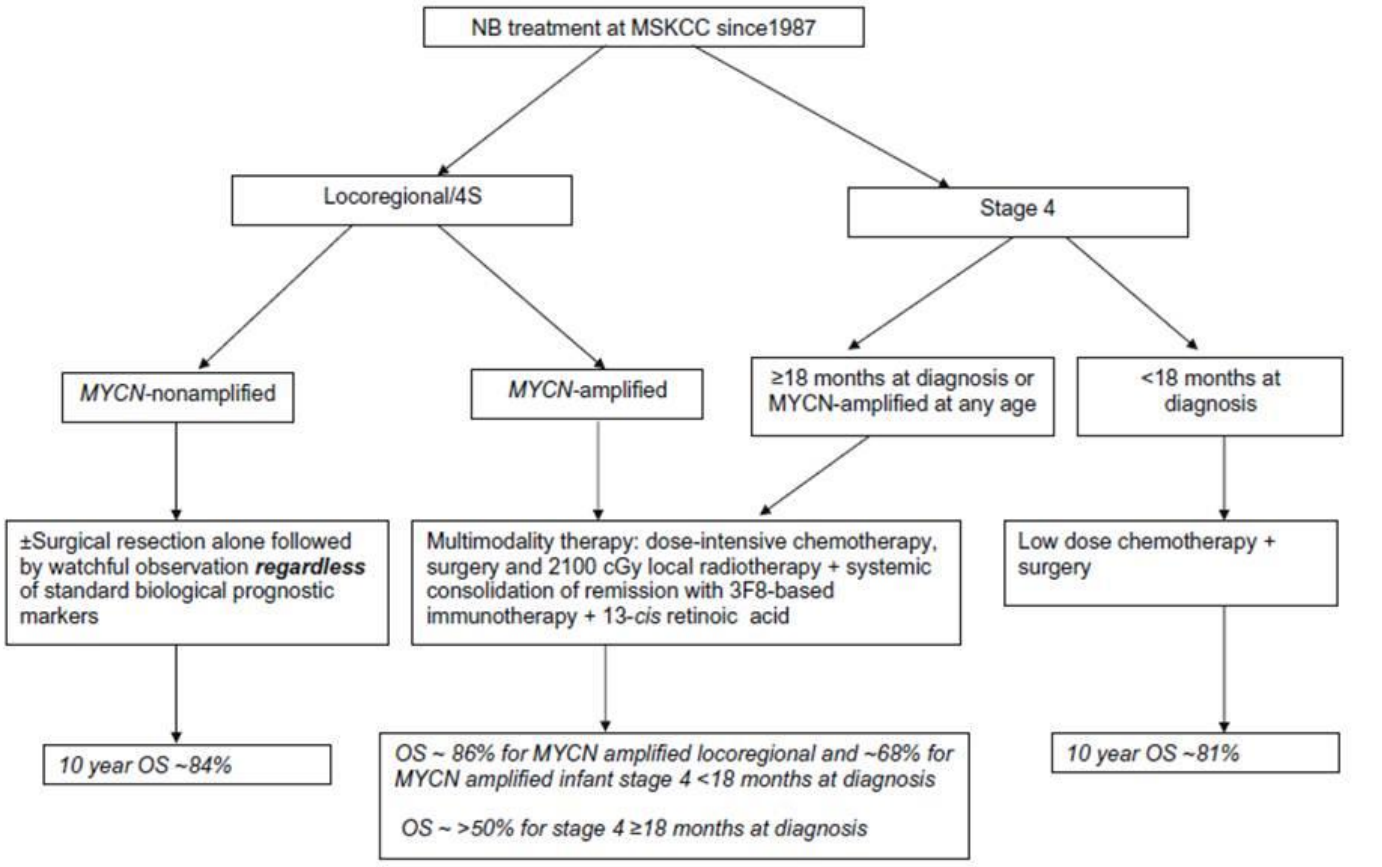

Figure 1-3. Possible treatment scheme for neuroblastoma[27].

OS: Overall Survival Rate.

Reprinted from Cancer Treatment Reviews, 36, Modak, S., and N. K. Cheung, Neuroblastoma: Therapeutic strategies for a clinical enigma/ Cancer in Childhood, Pages 307-317, Copyright (2010), with permission from Elsevier.

CHAPTER 2
IN VITRO ASSESSMENT OF MYXOMA VIRUS TREATMENT

Materials and Methods

Cell Lines

BSC-40 and SK-N-AS cells were maintained in Dulbecco's Modified Eagle Medium (DMEM) supplemented with 10% fetal bovine serum (FBS), 2 mM L-glutamine, and 100 U/ml of penicillin/streptomycin in a humidified chamber at 37°C and 5% CO_2. The human derived-neuroblastoma cell line, SK-N-AS, was obtained from the American Type Culture Collection (ATCC® CRL-2137™). The BSC-40 monkey kidney cell line was received as a gift from Richard Condit within the University of Florida College of Medicine. During maintenance, cell cultures were periodically tested to confirm the absence of contaminating mycoplasma species, using a PCR-based assay (Southern Biotech #13100-01).

Myxoma Virus and Viral Infections

This laboratory has previously described the Lausanne strain Myxoma Virus, which expresses green fluorescent protein at an intergenic location in the viral genome, under control of a synthetic viral early/late promoter (vMyx-eGFP) [33]. This vMyx-eGFP virus is used in all experiments, with the exclusion of the viral binding assay. Also described elsewhere is vMyx-Venus/M093, which contains an (N)-terminal Venus-fused M093 protein (Lausanne) [9]. This allows for the detection of fluorescent virus particles as they attach to host cell surfaces. All viral stocks were propagated and titrated in BSC-40 cells. Virus was purified through a 36% sucrose cushion according to standard laboratory protocol[34]. For infection, cells were exposed to virus at a MOI dependent on

experimental conditions. Incubation with virus occurred in one of two ways: 1) by mixing cells in suspension with viral inoculum or 2) by the overlay of liquid viral inoculum on adherent cells. This allowed for the comparison of different viral adsorption methods and their effect on experimental outcomes. When infection was completed on adherent cells, cells were then released from culture dishes by 0.025% Trypsin-SSC, and used to complete experiments. Unless otherwise indicated, infections were carried out for one hour in supplemented DMEM + 10% FBS in a humidified chamber at 37°C and 5% CO_2. Mock controls were not exposed to Myxoma Virus. Instead, cells were treated with supplemented DMEM + 10% FBS under the same conditions as virus-treated cells.

Analysis of Viral Infection by Fluorescent Microscopy

For infection, SK-N-AS and BSC-40 cells were seeded for confluence in tissue culture dishes. On the following day, cells were adsorbed with vMyx-eGFP for 1 hour and the infection was allowed to proceed overnight. The ability of the virus to infect and spread among cells was observed at both high and low multiplicity of infection (10 and 0.1). Infected cells were imaged for eGFP fluorescence over a period of three days at 50X magnification. Fluorescence and phase-contrast images of cells were captured using a Leica DMI6000 B inverted microscope. Images were minimally processed and pseudocolored using Adobe Photoshop software (Adobe Systems).

Observation of Viral Replication in Cell Cultures

Confluent monolayers of BSC-40 and SK-N-AS (on 12-well plates) were infected with vMyx-eGFP for one hour at 37°C. Afterwards, cells were washed 3X with room temperature PBS to remove excess virus and overlaid with liquid medium. Cells were harvested at the indicated hours post infection (hpi), pelleted, and frozen (-80°C). Infectious material was released from cells by three sequential freeze-thaw cycles and

sonication. The amount of virus in cell lysates of individual samples was determined by foci formation in BSC-40[34]. Comparison of vMyx-eGFP replication in BSC-40 and SK-N-AS was performed in a single experiment at a MOI of 5. Independently, one-step (MOI 5) and multi-step (MOI 0.1) growth curves were completed in SK-N-AS over three separate experiments.

Assessment of Cell Proliferation and Viability

For preparation, cells were seeded on 6-well plates in triplicate. Various cell concentrations were plated, depending on cell type and experiment. On the following day, adherent cells were either mock-treated or infected with vMyx-eGFP (MOI 10). Beginning on Day 1, the numbers of viable cells were counted daily on a hemocytometer according to trypan blue-exclusion. Overall, cell viability assays were carried out more than once. There were two independent experiments performed in BSC-40 (with $3x10^3$ or $5x10^3$ adherent cells treated) and three experiments for SK-N-AS (between $5x10^3$and $9x10^4$ adherent cells treated). Cell viability rates were calculated according to: the viable cell count per day, divided by the number of input cells that were treated on Day 0. From this, average percent viability was used to normalize viable cell counts for $2x10^3$ cells.

Determination of SK-N-AS Colony Forming Ability

Immediately prior to treatment, SK-N-AS cells were released from tissue culture dishes by 0.025% Trypsin-SSC. Cells in suspension were then treated for one hour at 37°C with vMyx-eGFP or Mock. Two independent experiments (Trial 1 and Trial 2) were performed, with details included below.

Trial 1

There were $1x10^7$ cells suspended in a total volume of 300ul of the viral inoculum ($3x10^4$ cells per ul, MOI 10 or 0). Serial dilutions were performed and cell concentrations of 10^6 through 10^1 were seeded on 6-well plates in duplicate. Cells were maintained in culture and at 14 days post infection the number of colony forming units (CFU) counted manually.

Trial 2

Three independent SK-N-AS cell populations (A, B or C) were incubated with vMyx-eGFP (MOI 10, 3, 1, 0.1 and 0). Each group of $1x10^4$ cells was suspended in a total volume of 20ul for treatment ($5x10^2$ cells per ul). Serial dilutions were performed and cell concentrations of 10^3 through 10^1 were seeded in 6-well plates, to allow growth for 10 days. Cells were examined for CFU on the 10^{th} day after initial infection. On the 13^{th} day, growing colonies were challenged with a second dose of vMyx-eGFP (MOI $\geq$ 200) to test for resistance to MYXV. Four days later, media was removed from culture dishes, cells were rinsed 1X with SSC to remove excess virus/dead cells, and media was replaced for the final counting of CFU. The calculation of MOI for secondary challenge with virus was based on $1x10^4$ cells per treatment group.

Analysis of Myxoma Virion Binding to Cells

On the previous day, cells were seeded at confluence in 24-well plates. For suspension-treated groups, cells were detached from tissue culture plates using 0.025% Trypsin–SSC immediately prior to binding. To allow virion attachment to cells, vMyx-Venus/M093 was incubated with BSC-40 and SK-N-AS at a MOI of 20. The incubation period was carried out at 4°C for one hour. After adsorption, cells were washed 3X with chilled PBS to remove unbound virus. Cells were fixed in 4 % paraformaldehyde–PBS

and analyzed using a BD FACSCalibur apparatus (BD Biosciences) for flow cytometry. Data shows results from a single experiment.

Results

Background

The poxvirus, Myxoma Virus, replicates exclusively in the cytoplasm of permissive cells. Under fluorescent microscopy, the initiation of gene expression by vMyx-eGFP is visible according to green fluorescence in cultured cells. This is because green fluorescent protein is transcribed under the control of a viral promoter that is engineered to be active during both early and late stages of the MYXV life cycle. The successful completion of the replication cycle is assessed by the generation of new infectious progeny virus as assessed by titration on susceptible indicator cells. At a high multiplicity of infection (MOI), individual virus particles are added in excess of the number of cells in order to infect the majority of the test cells. This is referred to as a single step growth curve. In low MOI infections, the ratio of viral foci forming units (FFU) per cell is lower, such that each cell comes into contact with less than one virus particle, on average. This allows for the assessment of the capacity of the virus to be spread from cell-to-cell at the end of the replicative cycle. BSC-40 monkey kidney cells are highly permissive to MYXV infection and are used as a positive control. The human-derived neuroblastoma cell line, SK-N-AS, is used to investigate the impact of MYXV on neuroblastoma cell behavior.

Myxoma Virus Infects and Spreads Successfully in Cultured SK-N-AS Cells

To visualize infection, SK-N-AS cells, a human cell line derived from a high-risk neuroblastoma patient, were seeded onto cell monolayers and adsorbed with vMyx-eGFP at a MOI of 10 FFU per cell. Infection of SK-N-AS results in high levels of GFP

expression that is visible in the majority of cells and was similar to infection of BSC-40. The virus also changes the normal morphology of SK-N-AS by causing cells to recede from the surface of culture dishes, disrupting cell-cell contacts within the monolayers, and visibly reducing the amount of adherent cells present in comparison to non-virus controls (Figure 2-1, A-F). The observation of SK-N-AS monolayer infection at 0.1 MOI was continued over three days. Twenty-four hours after infection, visible GFP was limited to individual cells in a low percentage of the total population. During the following days, levels of GFP fluorescence increased by viral spread to adjacent cells. This occurs as centers of viral replication, as measured by the increase in GFP levels, grow to form foci of larger size (Figure 2-1, G-I).

SK-N-AS is Permissive for Myxoma Virus Replication

Growth curve experiments provide a better understanding of viral replication in SK-N-AS cells. In a single-step growth curve at high multiplicity of infection (MOI 5), maximal viral yields of replication are indistinguishable between BSC-40 and SK-N-AS cells. The amount of infectious virus generated in the neuroblastoma cells at early time-points apparently lags when compared to the BSC-40 cells. However, this difference is no longer detected by 24 hours post infection (Figure 2-2A). In addition, three independent growth experiments were repeated to confirm that vMyx-eGFP undergoes a fully productive growth cycle in SK-N-AS. Permissive levels of viral replication are observed with reproducibility in both one-step and multi-step growth curves. Finally, multi-step growth experiments confirm the earlier observation that MYXV is able to spread cell-to-cell, since a low amount of input virus on cell monolayers is able to increase exponentially over time (Figure 2-2B).

Myxoma Virus Infection Kills SK-N-AS Cells

Both BSC-40 and SK-N-AS exhibit immortality *in vitro* and logarithmic growth. However, when adherent cells are infected with vMyx-eGFP (MOI 10), the virus interrupts normal cell proliferation. This occurs with different viability results for each cell type. MYXV treatment of BSC-40 prevents further outgrowth of this cell line in culture (Fig 2-3A). In SK-N-AS, MYXV infection comparably reduces the total number of viable cells that are capable of further cellular divisions (Fig 2-3B). Cell viability is calculated according to: the viable cell count per day, as assessed by trypan blue exclusion of living cells, divided by the number of input cells that were initially infected. Accordingly, MYXV-treatment kills 80% of the initial SK-N-AS cell population by the sixth day after infection (Fig 2-3C). In the neuroblastoma cell line, Myxoma Virus induced death first appears at two days, before more extensive cell death ensues in subsequent days. This supports that viral replication within SK-N-AS initially proceeds more slowly than in BSC-40 cells, as was observed in the single step growth curve experiments.

Myxoma Virus Inhibits SK-N-AS Colony Formation

Another way to assess cell proliferation is to plate a low concentration of cells, so that they are individually distributed throughout the culture dish without touching any adjacent cells. As cell numbers double over time, this leads to the formation of distinct colonies that have each initiated from one cell. In these experiments, SK-N-AS cells were first brought into suspension and then adsorbed with viral inoculum prior to culturing in monolayers for two weeks. When a high concentration of SK-N-AS ($3x10^4$ cells per ul) is adsorbed with a small inoculum volume containing 10 FFU per cell, SK-N-AS colony formation is reduced to 3% of the non-virus control cells (Fig 2-4A).

Adsorption Conditions are Important for MYXV Cell Killing Efficiency

Figure 2-4A also shows that vMyx-eGFP inhibition of cell colony formation is dependent on both the total volume of viral inoculum and the multiplicity of infection. With a lower ratio of cells per inoculum volume ($5x10^2$ cells per ul) the same MOI of 10 only reduces colony formation by 53%. We observe increasing numbers of colony forming units (CFU) that survive MYXV-treatment, along with decreasing FFU per cell. At the very least, this decrease in MYXV cell killing efficiency is seen at a MOI of 3 and lower (intermediate MOIs were not tested).

Suboptimal adsorption conditions mean that not all cells are exposed to sufficient MYXV to initiate infection. Under these initial binding parameters, 47% of cells will continue to grow out in culture, including those exposed to a low dosage of virus. Out of all cell colonies still growing in culture at 10 days post infection, 1% of these were found to express GFP (Fig 2-4B and Table 2-1). These GFP colonies were found within all three SK-N-AS sub-populations in Trial 2 and occurred more frequently at higher multiplicities of infection (Table 2-2). Secondary challenge with vMyx-eGFP at $\geq$200 FFU per cell, shows that these colonies are not resistant to MYXV infection, as none survived secondary treatment (Fig 2-4C). The scrutiny of SK-N-AS cultures at 4 days post MXYV-challenge revealed that only one small subset of cells could be found remaining. This minority of adherent cells was greatly diminished in number and lacked the flat cell morphology characteristic of normal growth in mock-treated colonies (Fig 2-4D). We conclude that the cells surviving the first exposure of MYXV were not selected as resistant clones, but rather had likely not been adsorbed with sufficient virus to initiate a productive infection following the initial virus binding protocol.

Myxoma Virus Binds More Efficiently to Cells in Suspension

Myxoma Virus particles have previously been made directly detectable through the fusion of fluorescent Venus to the MYXV virion M093 protein, in frame to the N-terminus of the open reading frame[9]. Because M093 is a member of the viral protein core, vMyx-Venus/M093 virions thus are fluorescent and their binding to mammalian cells can be assessed by flow cytometry. The equivalent replication features of vMyx-Venus/M093 and vMyx-eGFP have already been established[9]. The incubation of vMyx-Venus/M093 with cells at 4°C arrests the procession of virus infection at the fusion/entry step of the replication cycle, so that we specifically can monitor virus attachment to cells. Virion binding efficiency was assessed for adherent cells and cells in suspension, according to Venus detection of virus-adsorbed cells by flow cytometry. Out of the total population, we observed a higher percentage of virus-bound cells for the suspension group and also a greater number of bound virions per cell (Fig 2-5).

Table 2-1. Frequency of SK-N-AS colonies in Trial 2 that still express GFP 10 days after infection

	Actual CFU	Expected CFU per $1x10^4$ cells
Visible GFP	21	500
% Occurrence	1 %	5 %

CFU: colony forming units

Table 2-2. Number of GFP-expressing colonies at each multiplicity of infection

	Group A	Group B	Group C	Average
MOI 10	4	5	1	3.33
MOI 3	1	7	0	2.67
MOI 1	1	1	1	1
MOI 0.1	0	0	0	0

All data is from CFU Trial 2, at Day 10 post infection
MOI: multiplicity of infection

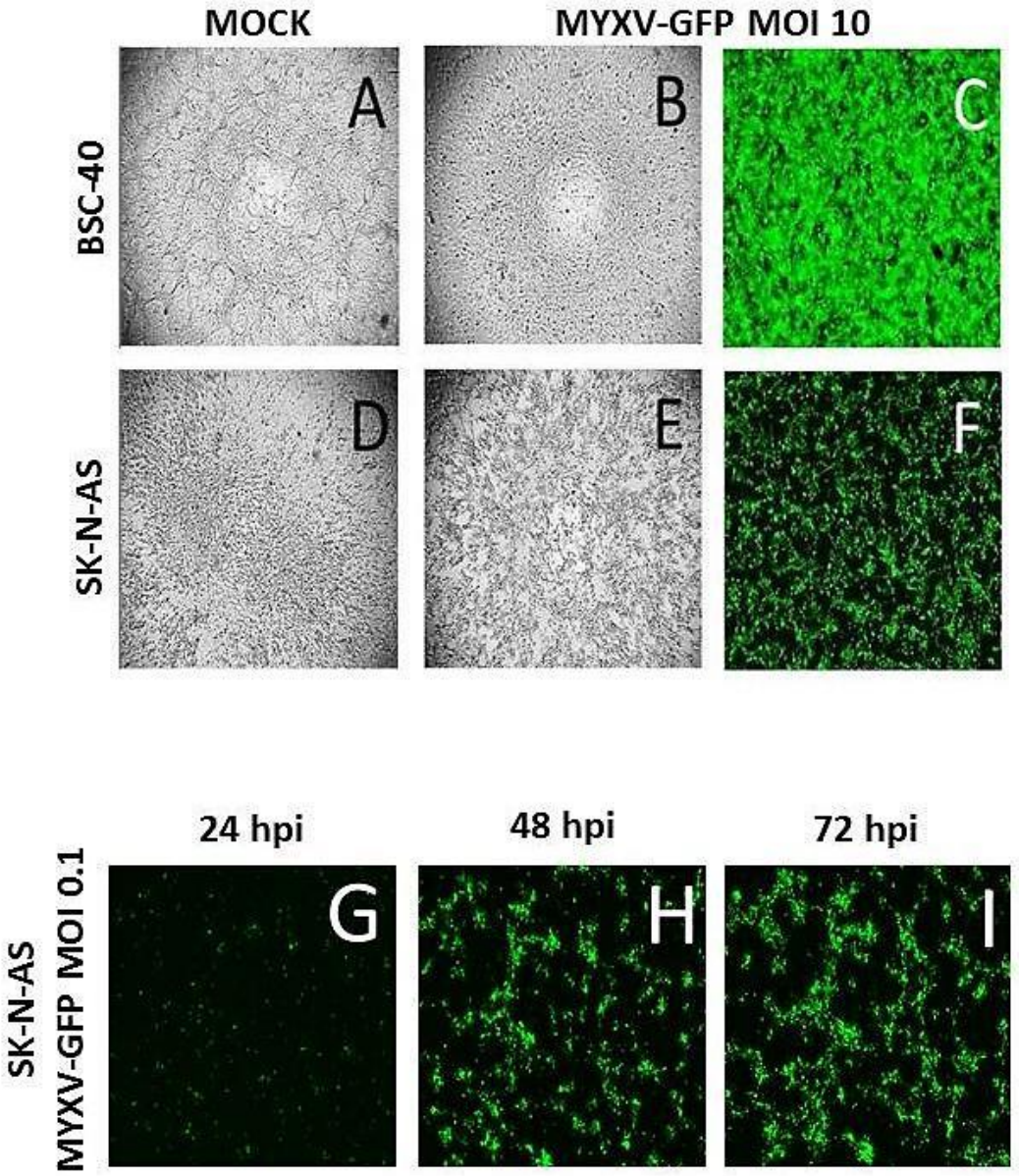

Figure 2-1. Myxoma Virus is able to infect the neuroblastoma cell line SK-N-AS. Cells were incubated overnight with vMyx-eGFP on confluent cell monolayers. The BSC-40 monkey-kidney cell line has been previously characterized as permissive to Myxoma Virus. A-F) Cells were infected at a high multiplicity of infection (MOI) of 10 to assess viral expression of eGFP. Myxoma Virus limits the growth of cells compared to overgrown mock cell cultures. E-F) MYXV causes abnormal cell morphology of SK-N-AS at a high MOI. G-I) Confluent SK-N-AS monolayers were infected with a low multiplicity of infection (MOI 0.1). Myxoma Virus is able to spread cell-to-cell and the foci of viral replication increase in size over time.

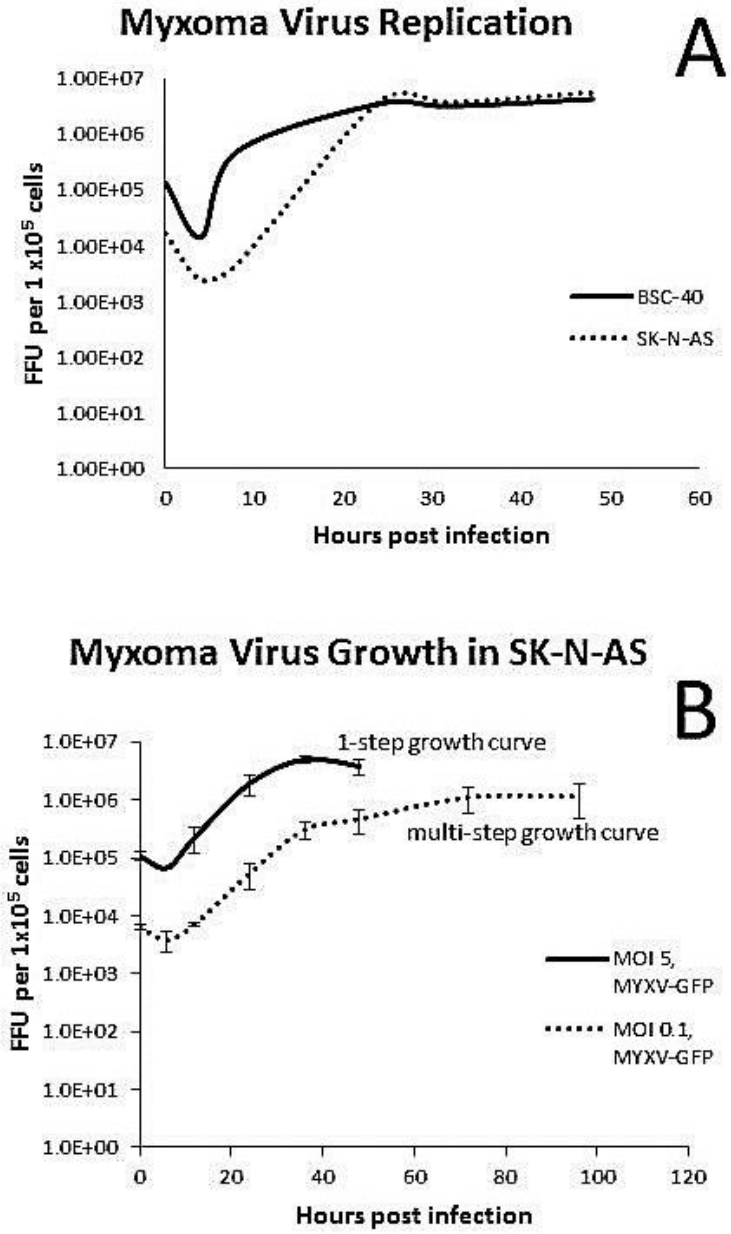

Figure 2-2. SK-N-AS is permissive to Myxoma Virus replication. A) In the one-step growth curve, cells were incubated for 1 hour with vMyx-eGFP at MOI 5. Samples were collected at indicated times to measure the amount of infectious virus particles present in cell lysates. For both BSC-40 and SK-N-AS, Myxoma Virus is able to replicate at comparable levels. B) Single-step and multi-step growth experiments were repeated three times in SK-N-AS to confirm observations. In the multi-step growth curve cells received a low amount of input virus, showing that when vMyx-eGFP replicates in SK-N-AS, the virus is able to reproduce itself and spread among cells.

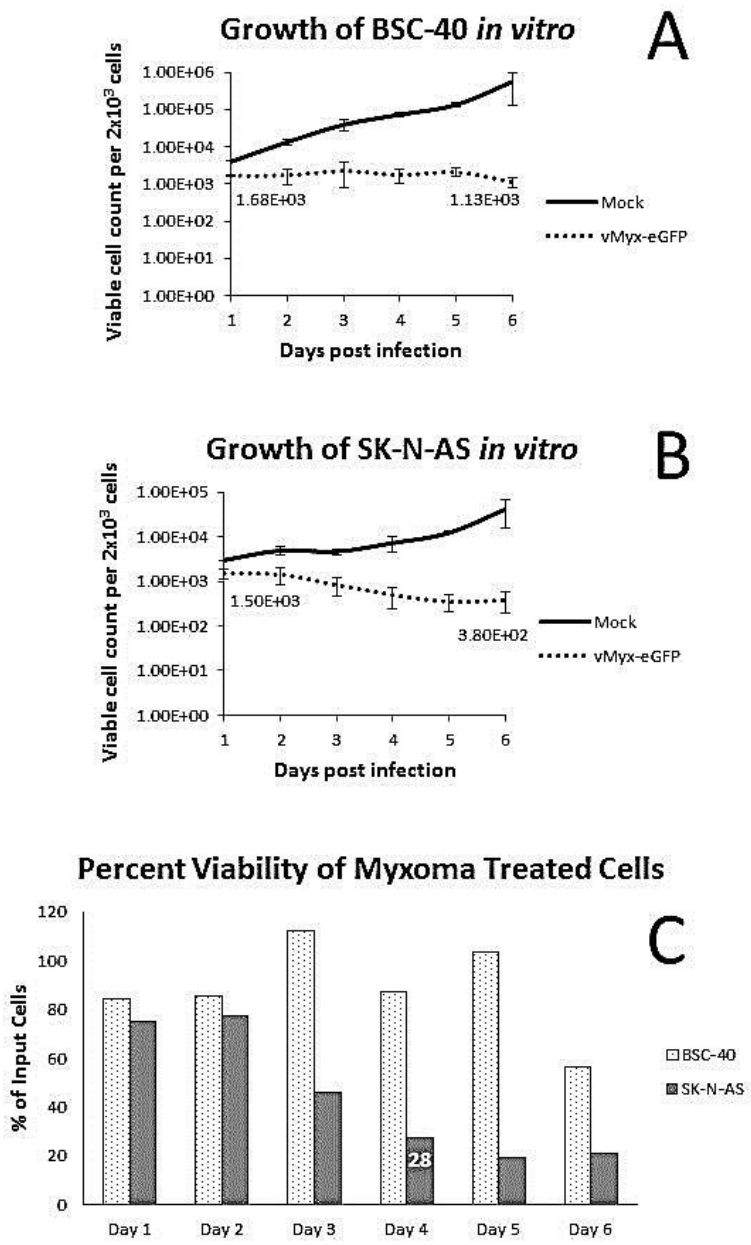

Figure 2-3. Myxoma Virus reduces cell viability *in vitro*. BSC-40 and SK-N-AS cells were seeded on culture dishes and infected the next day at MOI 10. Over the following period of 6 days, the numbers of trypan blue-excluding cells were counted manually on a hemocytometer. A-B) Adherent cells were incubated with vMyx-eGFP and cell proliferation in culture was reduced. C) Percent viability was calculated as: viable cell count per day, divided by the number of input cells infected on Day 0. MYXV prevents the outgrowth of BSC-40 cells. In SK-N-AS, MYXV kills 80% of the initial cell population by the sixth day of infection.

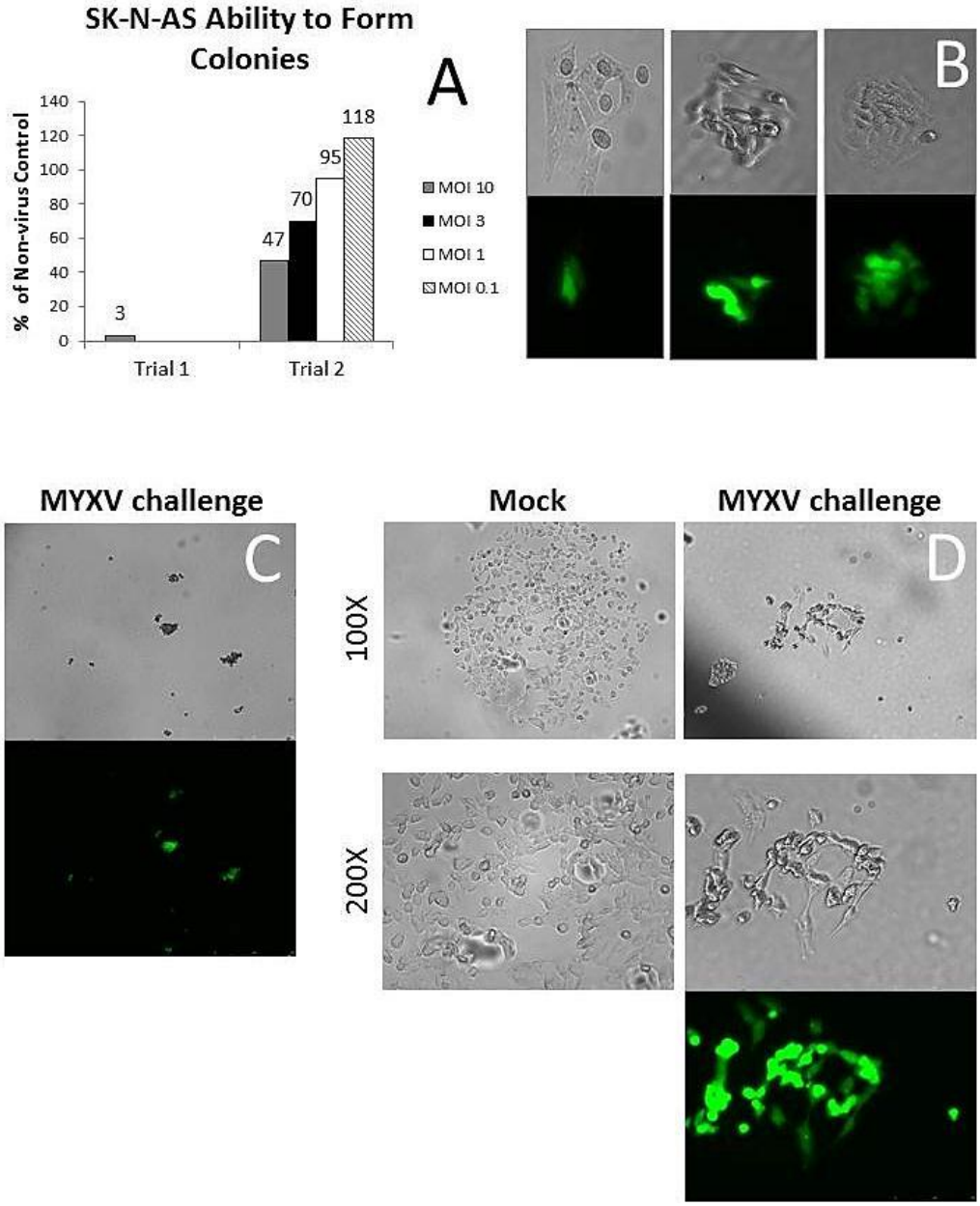

Figure 2-4. Myxoma Virus inhibits SK-N-AS colony formation. This inhibition of CFUs differs with incubation methods. A) SK-N-AS cells in suspension were incubated with vMyx-eGFP. Trial 1 and 2 differed in inoculum volume ($3x10^4$ cells/ul or $5x10^2$ cells/ul respectively). Treated cells were allowed to grow for 2 weeks in culture. B) Trial 2: out of all MYXV-treated colonies still growing in culture 10 days after initial infection, 1% express GFP. C) All colonies in Trial 2 were challenged with MOI $\geq$200 at 13 days post infection. Four days later, there were no colonies present in any MYXV treated samples. Images were taken at 50X magnification. D) After MYXV challenge, there is a patch of adherent cells still attached to the bottom of one culture dish. These cells are comparably reduced in number and appear more rounded than those within Mock colonies.

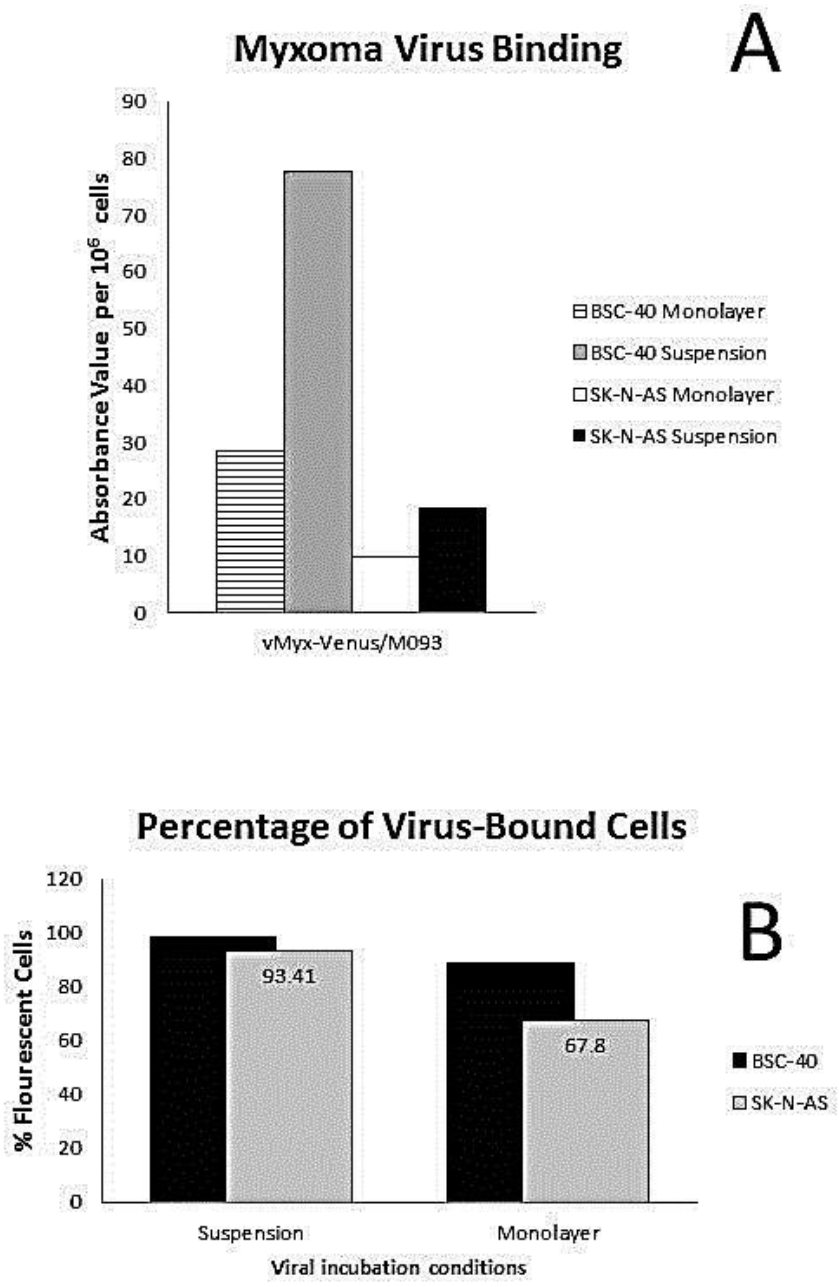

Figure 2-5. Binding of Myxoma virions differs with cell incubation conditions. Either adherent or suspended cells of BSC-40 and SK-N-AS were infected for 1 hour at 4ºC (vMyx-Venus/M093 MOI 20). Since virions are visible by fluorescence, measurements of virus-to-cell binding were collected by flow cytometry. Suspension-treated cells bind more individual virions and there are a higher percentage of virus-bound cells.

CHAPTER 3
MYXOMA VIRUS THERAPY FOR THE XENOGRAFT MODEL OF NEUROBLASTOMA

Materials and Methods

All animal experiments were carried out under approved University of Florida Institutional Animal Care and Use Committee protocol 2011-05023. NOD/Scid/IL2Rγ^{-02} (NSG) mice were obtained from the UF in-house breeding colony and provided with food and water *ad libitum*. To study SK-N-AS engraftment, 6 to 8 week old mice were injected intravenously via tail vein with cells in PBS + 10% FBS. The use of untagged SK-N-AS cells meant that engraftment levels and tumor development could only be visualized post-mortem. Before injection, cells were treated *ex vivo* for one hour at 37ºC (with either vMyx-eGFP or Mock). The NSG mice were humanely sacrificed when they reached a body condition score of 2, regardless of planned experimental endpoints[35]. Four to six weeks after xenotransplantation, all surviving mice were euthanized. Tissue samples were harvested from liver and lung (or kidney, and spleen in earliest experiments) followed by preservation in formalin and immunostaining against the human LAMP-1 membrane glycoprotein (BD Biosciences). The α-LAMP-1 antibody is an IgG isotype from BALB/c mice. All tissues were visualized under bright-field microscopy at the UF MBI Cell and Tissue Analysis Core (OLYMPUS IX70 for 20X, 40X and Zeiss Axioplan-2 for 50X, 100X magnifications). The conditional differences of each experiment are described below.

Maximum SK-N-AS Dosage in Sub-lethally Irradiated Mice (NSG Experiment 1)

Mice were sub-lethally irradiated using 175 cGy total body irradiation from a Cs^{137} source. Mice were injected with pre-treated SK-N-AS cells within 24 hours post irradiation. All irradiated animals received prophylactic antibiotics administered in the

water supply for 2 weeks post-transplantation (Baytril® 100, Bayer Healthcare). The infection of SK-N-AS occurred with cells in suspension ($1.6x10^4$ cells per ul) at a MOI of 10 or 0. After treatment, cells were released into suspension by 0.025% Trypsin-SSC and each animal received $2.86x10^6$ cells suspended in 100ul total volume for injection. This was followed by observation for six weeks. Animal cohorts of Mock and MYXV contained 5 mice each. There was also one untreated animal that did not receive SK-N-AS or vMyx-eGFP (for 11 NSG total). In addition to tissues listed above, bone marrow was collected from the right hind femur using a tuberculin syringe. These bone marrow samples were analyzed by flow cytometry for the detection of human HLA-A, HLA-B, and HLA-C (BD Biosciences).

SK-N-AS Dose De-escalation in Non-irradiated Mice (Preliminary Experiment)

Several factors were altered to determine optimal conditions for future experiments. To begin with, mice were not irradiated prior to tail vein injection. Treatment was also completed on adherent cells instead of cells in suspension. The multiplicity of infection for virus-treated cells was increased to 25. Serial dilutions were performed on treated cells prior to injection, to yield concentrations of $2x10^6$ through $2x10^1$ cells received per mouse. All cell concentrations were suspended in a final volume of 100ul per mouse for injection. Finally, mice were euthanized either at four or six weeks post injection. Cohorts of Mock and MYXV contained 12 animals each, with 2 mice at each SK-N-AS dilution (24 NSG total).

Various SK-N-AS Conditions in Non-irradiated Mice (NSG Experiment 2)

Pre-treated cells were administered to non-irradiated mice at different cell concentrations and injection volumes: $4x10^6$ cells in 100ul; $2x10^6$ cells in 50ul; $1x10^6$ cells in 50ul; $4x10^5$ cells in 30ul; and $2x10^5$ cells in 100ul. Multiple conditions were used,

as procedures still had not been optimized (at high concentrations of cells in large injection volumes, animals experienced health complications and were euthanized). At all cell concentrations, treatment of SK-N-AS occurred with incubation of vMyx-eGFP on adherent cells at a MOI of 10 or 0. Due to limited supply in the breeding colony, animal cohorts were uneven in number (9 Mock and 10 MYXV) for a total of 19 NSG mice. All surviving animals were euthanized and tissues harvested at 6 weeks post injection.

Final Purging Model in Sub-lethally Irradiated Mice (NSG Experiment 3)

Mice were sub-lethally irradiated, injected with pre-treated cells within 24 hours, and received prophylactics (as in NSG Exp 1). Animals received $2x10^5$ cells suspended in 50ul total volume. The *ex vivo* treatment of SK-N-AS was completed on adherent cells at MOI 10 or 0. Due to limited colony size, cohort groups were again uneven in number. There were 4 Mock-treated and 5 MYXV-treated, for 9 NSG total. All mice were euthanized and tissues collected during the 6^{th} week following injection (on day 45).

Tissue Analysis by Immunohistochemistry (IMHC)

Infiltration of human cells (SK-N-AS) into murine tissues and subsequent tumor development was analyzed by IMHC. Tissues were fixed in 10% formalin buffered with PBS for 48 hours and then soaked in 70% ethanol until encasement in paraffin. The embedding process and all immunohistochemistry were performed by the UF Molecular Pathology Core. Sections of formalin-fixed, paraffin-embedded blocks were cut and picked-up onto plus charged slides. Slides were de-paraffinized and rehydrated through a series of xylenes and graded alcohols and blocked with 3% peroxide/methanol. Heat mediated antigen retrieval was performed in Trilogy™ buffer (Cell Marque). This was immediately followed by blocking with normal goat serum and avidin/biotin. Mouse anti-huLAMP-1 was applied to sections for 1 hour at room temperature. Staining was

performed by the avidin-biotin complex method. Slides were counterstained with hematoxylin prior to coverslipping.

Determination of IMHC Agreement with Necropsy Observations

To test the accuracy of SK-N-AS detection, necropsy and IMHC observations were compared. This is called “IMHC agreement” and was determined as follows: 1) LAMP-1 staining was assessed for each individual animal; 2) Based on this, general predictions were made of whether SK-N-AS engraftment was high enough to result in a visible tumor that would have been noted during necropsy; 3) IMHC predictions were then compared to the actual counts of cancerous growths recorded during necropsy; 4) For each animal, it was determined if IMHC agreed with necropsy observations in none, both (liver and lung), or only one tissue. Since time of necropsy and IMHC analyses were separated by 2 to 4 weeks, the evaluation is not biased.

Summary of IMHC Results (NSG Experiment 3)

SK-N-AS engraftment was analyzed by histology: 1) in each animal, both liver and lung samples were processed by immunohistochemistry; 2) For each sample, four images from different areas of the tissue were taken under bright-field microscopy; 3) By visual comparison, images were placed into categories of likeness in staining patterns (similar engraftment levels) among animals of the same cohort; 4) From these:

- Images were observed for the presence of $\geq$1 LAMP-1 staining region. These were calculated as a percentage of tumor-free images (<1 LAMP-1 staining region) out of all sections per cohort (as in Tables 3-2 and 3-3), or
- For figures 3-7 and 3-8, categories of LAMP-1 staining patterns were sorted according to frequency of occurrence within all tissues of that treatment group, and one panel is shown as a representative of each of the engraftment categories, for 5 panels total.

Results

Background

The SK-N-AS cell line has been used to study tumor biology of neuroblastoma *in vivo* in immunodeficient animals[36, 37]. We have developed a model that examines the ability of MYXV to purge contaminating neuroblastoma cells from autologous stem cell transplant specimens. Thus, we have modeled this indication by the *ex vivo* treatment of SK-N-AS cells with Myxoma Virus, followed by tail vein injection of the treated cells into NSG mice. In this way, xenotransplantation is used as an assay to measure the ability of MYXV to eliminate or reduce the engraftment capacity of the neuroblastoma cell line. Higher oncolytic activity of MYXV will coincide with lower engraftment levels among the test animals. Up until our study, SK-N-AS has not been studied in this purging model. Therefore, this work included the preliminary study of cell engraftment, which then provided means for an assessment of the ability of *ex vivo* Myxoma virus treatment to alter such engraftment *in vivo.*

SK-N-AS Successfully Engrafts into Multiple Tissue Sites of NSG Mice

Tail vein injection causes detectable infiltration of SK-N-AS in multiple murine tissues harvested between four and six weeks. Tumors developed within body cavities that did not present as palpable during the lifetime of the animal. Cancerous growths in both liver and lungs were visible either during tissue dissection at necropsy or by α-LAMP-1 staining on formalin-fixed tissues. Summarized here are the results presented in Figure 3-1, which describe SK-N-AS xenotransplants in NSG mice. We observed varying levels of engraftment and the formation of different tumor forms (small cysts, solid tumors, and large necrotic tumors). This is apparent in the comparison of tissues harvested from different mice that received identical treatment. Disease spread also

varied within different tissues of an individual animal. Higher engraftment in the lung often, but not always, corresponded with lower engraftment in the liver of the same animal. The converse was also true. Finally, engraftment levels are not uniform throughout individual organs. This diversity occurs in different lobes of the liver or, as seen in Figure 3-1, in different sites of the lung. There was no detection of SK-N-AS tumor establishment in the bone marrow.

Appearance of Human LAMP-1 Staining Varies with Engraftment Levels

LAMP-1 antibody provides specific staining of human cells detected within NSG tissues, which exhibits little or no background levels in control mice. More often than not, LAMP-1 positive engrafted human tumor cells are easy to distinguish from the purple hematoxylin stain of normal murine tissue. However, LAMP-1 staining appears less intense (and more pink in color) in cases of relatively low SK-N-AS engraftment. This pale pink is a lighter derivative of the red-brown color that results from high infiltration and accumulation of SK-N-AS cells. When observing large areas of tissue at 50X magnification, it is easy to overlook the subtle difference between the less intense pink LAMP-1 staining and purple hematoxylin in liver tissues. The variation in staining is more visible within branching regions of the lung. Figure 3-2 further details this observation. It became increasingly important to consider this characteristic of LAMP-1 staining during histological analysis of engraftment, to avoid scoring false negatives.

SK-N-AS Tumors Grew More Aggressively in Sub-lethally Irradiated NSG Recipients than in Non-Irradiated Animals

In sub-lethally irradiated cohorts, animals displayed distinct phenotypes, according to tumor cell engraftment and progression of disease (Table 3-1). However, SK-N-AS engraftment levels were noticeably lower in the non-irradiated treatment

groups. In the Preliminary Experiment with non-irradiated mice, there were no abnormal phenotypes seen at necropsy and histology showed minimal staining within tissues harvested at 4 weeks. In these cohorts, engraftment preferentially favored lung tissues. Furthermore, injection of $2x10^4$ or fewer SK-N-AS cells per mouse was not detected when samples were collected as soon as 6 weeks later in non-irradiated mice. In NSG Exp 2, non-irradiated mice that received higher concentrations of input SK-N-AS cells still induced lower engraftment than irradiated mice harvested at similar time points (Fig 3-1, G-H). Finally, only sub-lethally irradiated mice exhibit symptoms of late disease onset that serve as signs for final stages of acquired disease. This phenotype and extreme sickness was not observed in non-irradiated animals.

MYXV Treatment Reduces Progression to Severe Disease

Pre-treatment with vMyx-eGFP consistently decreased SK-N-AS levels of engraftment in mice. In NSG Exp 1, the survival levels of MYXV-treated mice were increased over Mock by 4 to 8 days (Fig 3-3). This occurred along with visible reduction in tumor engraftment observed by histology (Fig 3-4). In experiments involving sub-lethally irradiated mice, the severe disease phenotypes of darkened skin, swollen abdomen, and reduced activity did not occur within MYXV-treated animals. These disease phenotypes were only observed within 1 to 2 days before full deterioration of animal health, meaning that MYXV treatment slowed disease progression. In the Preliminary Experiment with non-irradiated mice, MYXV treatment reduced LAMP-1 staining by levels comparable to 1 log difference (Fig 3-5 and 3-6). Additionally, clear differences in histology and necropsy images from NSG Exp 1, 2, and 3, suggest that MYXV elimination of SK-N-AS engraftment is actually much greater.

Results from NSG Exp 3 provide a comprehensive picture of the impact that *ex vivo* MYXV treatment has on subsequent SK-N-AS engraftment. Overall, histology images from MYXV-treated tissues were found to be tumor-free in 45% (liver) and 65% (lung) of all tissues. For animals not receiving MYXV, only 6.25% of liver tissues and none of the lung tissues were void of tumor-staining regions. Figures 3-7 and 3-8, are arranged such that each panel represents a category of SK-N-AS engraftment. Among animal cohorts, the frequency of occurrence for each engraftment level is reflected by the percentage of images that are similar in appearance. Here, immunohistochemisty reveals that the highest engraftment levels within MYXV cohorts were visibly lower than the highest engraftment in Mock. On average, MYXV treatment caused a massive reduction of SK-N-AS infiltration, compared to non-virus treated controls. In addition, images taken at the time of necropsy confirm these observations (Figures 3-9 and 3-10). However, in histology, it was noticeable that the current MYXV-treatment did not completely eliminate SK-N-AS engraftment, as varying regions of purple and pink staining still persist within the most reduced tissues. Tables 3-2 and 3-3 provide a summary of the histology results acquired from both NSG Experiment 3 and the Preliminary Experiment.

IMHC Disagreement Occurs within One Tissue 52% of the Time

Since SK-N-AS cell presence in murine tissues was detected by two methods (examination at necropsy and microscopic review of tissue sections), we compared the confirmation of SK-N-AS engraftment in both. This is called “IMHC agreement” when the two methods agreed. Out of all animals in NSG Exp 2 and 3, we see that IMHC agrees with necropsy results in both liver and lung tissues about half of the time and IMHC agreement only occurred for one of the two tissues the rest of the time. There

were no cases where IMHC disagreed with necropsy results in both lung and liver tissues of the same animal. Tables 3-4 and 3-5 show corresponding histology and necropsy images of those animals presented in Figures 3-1, 3-9, and 3-10.

Preferred Methods for Defining Levels of Engraftment Differed Between Liver and Lung Tissue Types

Sixty-two percent of all IMHC disagreements resulted from analyzing lung tissues during necropsy. The small size of murine lungs and light color of the tissue, made it difficult to visualize individual tumors at the time of necropsy. Even when IMHC can be used to successfully confirm necropsy assessment, observations taken at time of death do not accurately reflect the frequently low levels of SK-N-AS engraftment in the lungs. While this is true for any tissue type, these lower engraftment levels occurred more often in lung rather than liver samples. In addition, SK-N-AS infiltration in the lungs can result in flat growths that do not project off the surface and were difficult to see and score.

The primary complication experienced during dissection of the liver, is that tumor growths may be hidden within folds of the tissue, leading to false negatives. Out of 25 observations of liver at necropsy, cases of false negatives occurred twice (both of these were in NSG Exp 3). Other misinterpretations of liver tissues at necropsy occurred during the earlier NSG Exp 2 and the frequency of these decreased to zero with the acquisition of better technique and increased experience at scoring positive specimens. On the other hand, visualization of fluid-filled tumors and extremes at high or low engraftment levels are difficult to assess by histology in the liver. On the other hand, visualization of fluid-filled tumors and extremes at high or low engraftment levels are

difficult to assess by histology in the liver. Currently, the most reliable methods of analyses were found to be IMHC for lungs and necropsy observations for liver.

Table 3-1. Visible phenotypes observed at time of necropsy in NSG EXP 1 sub-lethally irradiated mice injected with maximal SK-N-AS dosage

Mice phenotype	+ NB - MYXV	+ NB + MYXV	- NB - MYXV
Darkened skin	5/5	3/5	0/1
Early euthanasia	3/5	0/5	0/1
NB Liver High	1/5 ***	0/5	0/1
NB Liver Medium	--	3/5	0/1
NB Liver Low	--	2/5	0/1
NB Lung	1/5 ***	0/5	0/1
NB Bone Marrow	0/5 ***	0/5	0/1

All animals received $2.86x10^6$ of the NB cell line, SK-N-AS
NB phenotype: SK-N-AS growths were visible/detected at necropsy
MYXV: treatment included viral adsorption in suspension, MOI 10
*** = Out of 5 animals, 3 were sacrificed early for humane reasons and these were not able to be viewed. Of 2 mice examined, one did not display signs of cell engraftment.

Table 3-2. Percentage of histology sections observed as tumor-free in NSG EXP 3

ex vivo Treatment	# Cells Injected	% Tumor-Free Sections LIVER	% Tumor-Free Sections LUNG	Irradiated?	Euthanasia
Mock	2×10^5	6.25 %	0 %	YES	6 wpi
MYXV	2×10^5	45 %	65 %	YES	6 wpi

Mock: treatment + NB – MYXV (MOI 0)
MYXV: treatment + NB + MYXV (MOI 10) viral adsorption on adherent cells
wpi: weeks post injection (treated cells administered by tail vein injection)

Table 3-3. Average number of cancer-staining foci per histology section in Prelim EXP

ex vivo Treatment	# Cells Injected	# Cancer Foci LIVER	# Cancer Foci LUNG	Irradiated?	Euthanasia
Mock	2×10^6	1.875	81.5	NO	4 wpi
Mock	2×10^5	0.25	3.2	NO	4 wpi
MYXV	2×10^6	0.5	4.75	NO	4 wpi

Mock: treatment + NB – MYXV (MOI 0)
MYXV: treatment + NB + MYXV (MOI 25) viral adsorption on adherent cells
wpi: weeks post injection (treated cells administered by tail vein injection)

Table 3-4. Number of tumors visible at necropsy in NSG EXP 2 non-irradiated mice, which received various dosages of SK-N-AS

Sample Name and Treatment	# Cells Injected	# Tumors Visible at Necropsy LIVER	# Tumors Visible at Necropsy LUNG	IMHC Agreement
NB6 Mock	4×10^6	10	ttc	II
NB7 Mock	2×10^6	12	ttc	II
NB8 Mock	2×10^6	1 *	ttc	I
NB9 Mock	2×10^5	2 *	0	I
NB10 Mock	2×10^5	2	0	II
NB11 Mock	2×10^5	1 *	0	I
NB12 Mock	2×10^5	0	0	II
NB13 Mock	2×10^5	3	0 *	I
MV6 MYXV	1×10^6	4	0 *	I
MV7 MYXV	1×10^6	0	0	II
MV8 MYXV	1×10^6	2	0 *	I
MV9 MYXV	4×10^5	3	0 *	I
MV10 MYXV	4×10^5	0*	0	I
MV11 MYXV	4×10^5	1	0 *	I
MV12 MYXV	4×10^5	0	0	II
MV13 MYXV	4×10^5	0	0	II

Table 3-5. Number of tumors visible at necropsy in NSG EXP 3 sub-lethally irradiated mice, which received $2x10^5$ SK-N-AS per animal

Sample Name and Treatment	# Tumors Visible at Necropsy LIVER	# Tumors Visible at Necropsy LUNG	IMHC Agreement
NB1 Mock	ttc	0 *	I
NB2 Mock	ttc	4	II
NB3 Mock	ttc	ttc	II
NB4 Mock	ttc	ttc	II
MV1 MYXV	4	0 *	I
MV2 MYXV	1	4	II
MV3 MYXV	3	0	II
MV4 MYXV	0 *	0	I
MV5 MYXV	0 *	0	I

For Tables 3-4 and 3-5:
Mock: treatment + NB – MYXV (MOI 0)
MYXV: treatment + NB + MYXV (MOI 10) viral adsorption on adherent cells
IMHC: agreement in one (I) or both (II) tissues
ttc: too many to count
* = necropsy and IMHC observations disagreed for this tissue
(NB denotes sample name only and not growth phenotype)

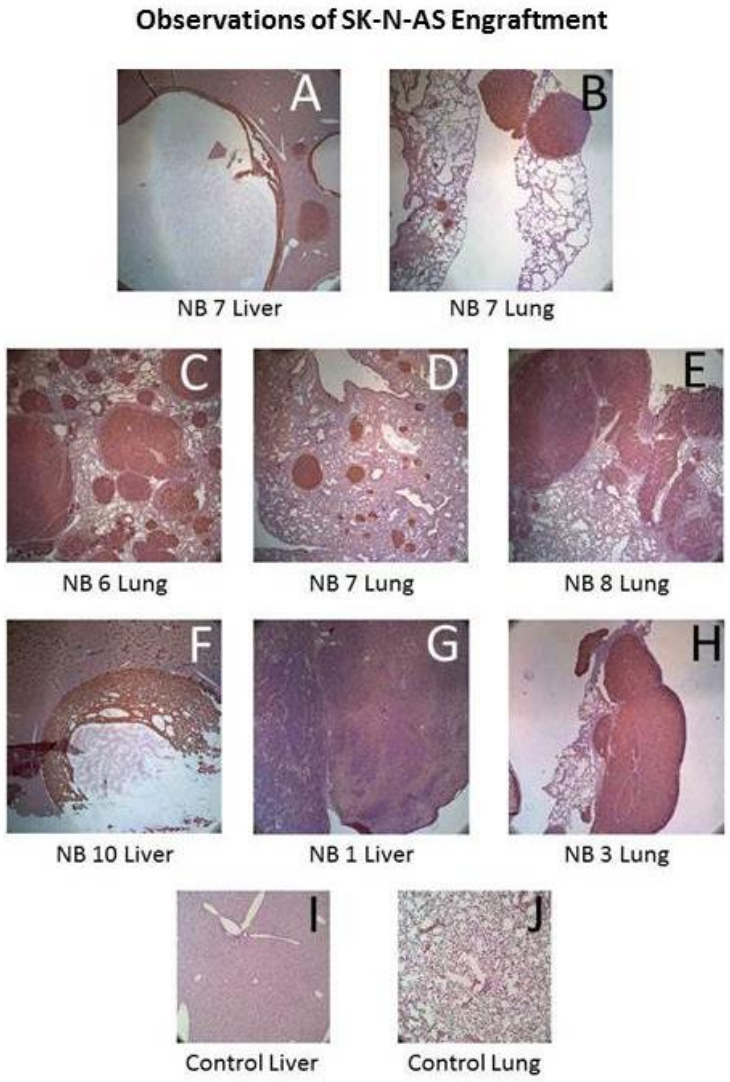

Figure 3-1. Different types of cancerous growths formed by SK-N-AS engraftment in NSG mice. A) Here the perimeter of brown, LAMP-1 stained cells indicates that a necrotic tumor was once present in the murine liver tissue; B) localized growth of SK-N-AS leads to the formation of two solid tumors in murine lung tissue. A-B) Both samples are from NB7 and we see that the diversity of growth types can occur within different tissues of the same animal. C-E) Levels of SK-N-AS engraftment also vary among animals of the same cohort. Histology is shown here as a strong method of analysis for murine lung tissues. F-G) For large growths occurring in the liver, histological review is possible but does not provide comprehensive assessment of the entire organ. It is also difficult to view cystic and necrotic growths. G-H) SK-N-AS engraftment occurs at higher rates in sub-lethally irradiated animals: NB1 and NB3 received $2x10^5$ cells after irradiation, but show higher engraftment than non-irradiated animals which received equal (NB10) or greater numbers of cells (NB6, NB7, NB8). Immunostaining was performed against huLAMP-1 glycoprotein. Images of treated samples are 50X magnification, controls at 40X. All sample names correspond with those in Table 3-4.

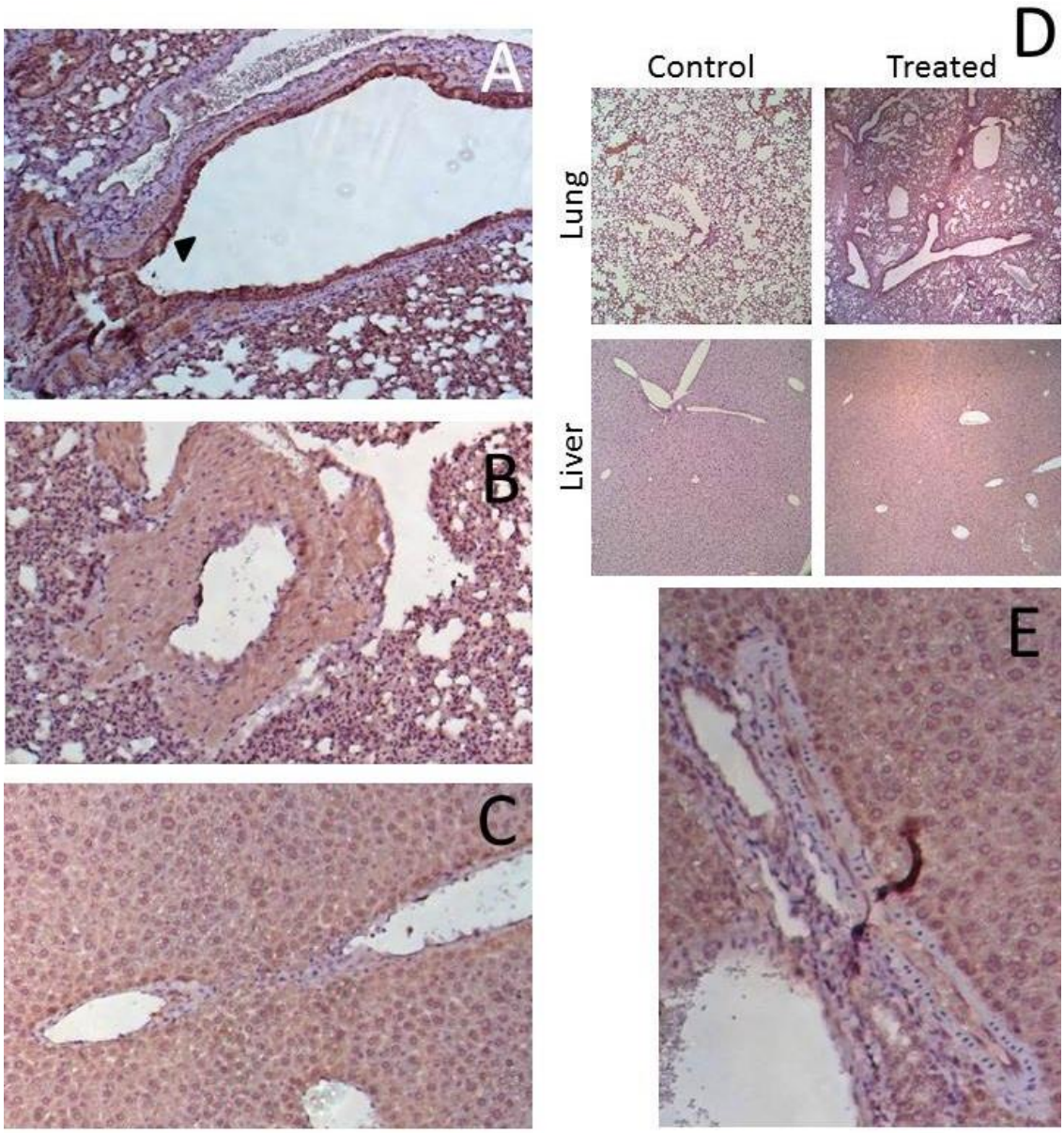

Figure 3-2. Appearance of α-LAMP-1 staining for varying engraftment levels of tumor cell engraftment. In tissues with less engraftment, staining appears pink instead of brown. A-B) Samples are from lung tissues. Murine cells appear purple; at low concentration SK-N-AS pink; and brown in areas of high SK-N-AS infiltration. The arrowhead in Figure A points to a region with alternating layers of brown, pink, and purple. D) Comparison of control and treated samples shows differential staining in lungs (alternating regions of pink and purple). This distinction is less apparent in liver samples, except for sites in the tissue where normal murine tissues remain isolated (C and E). Cell size and nuclei are visibly different in cells which stain pink (SK-N-AS) vs. purple. Variation in the appearance of stained cells is important in the consideration of overall engraftment levels that is assessed in the following experiments. The magnification of treated samples was 50X, and 40X magnification for controls. A, B, C and E are zoomed in.

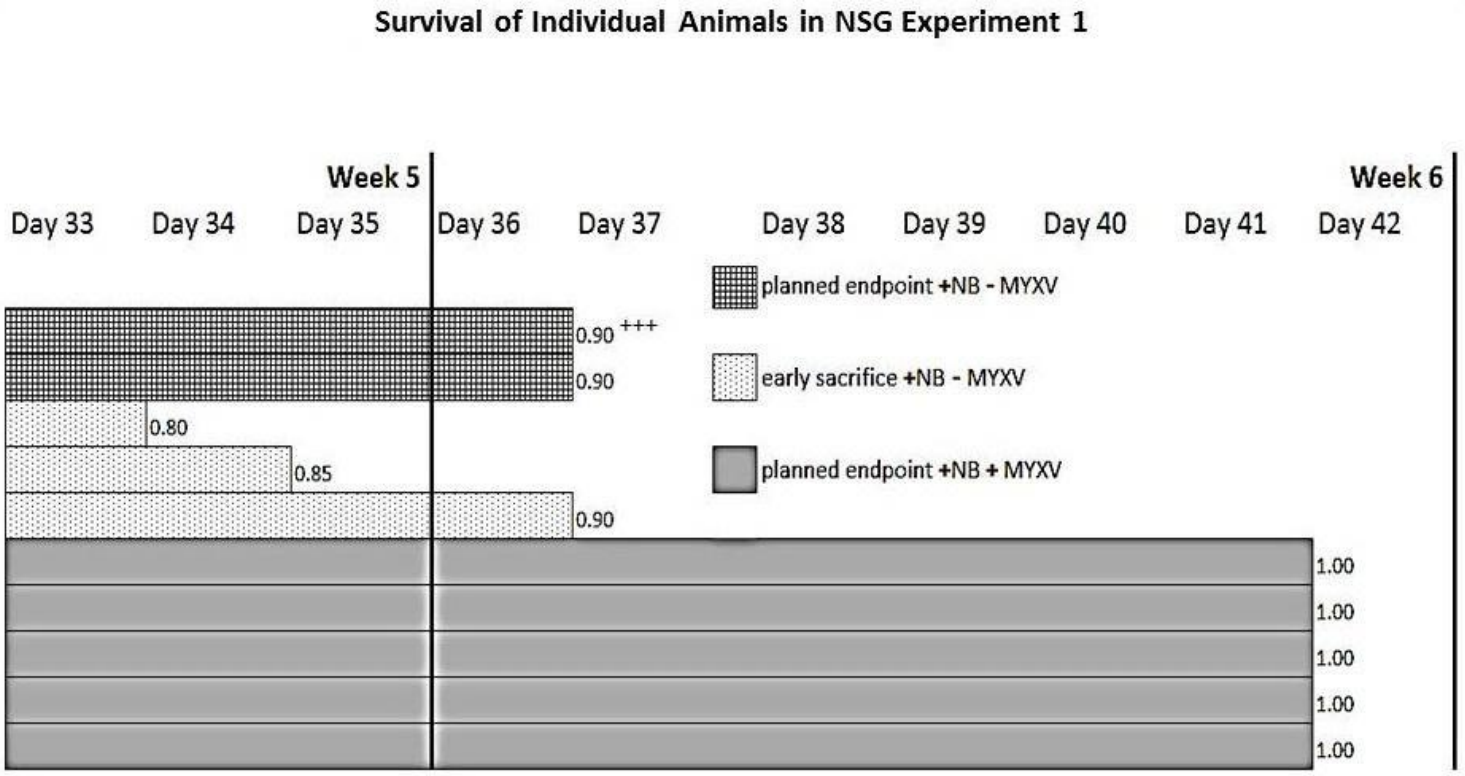

Figure 3-3. MYXV treatment of SK-N-AS extends survival of irradiated NSG mice. Each animal received $2.86x10^6$ cells intravenously. Prior to injection, suspended SK-N-AS cells were treated with vMyx-eGFP (MOI 10 or 0) for 1 hour. For those animals with successful engraftment, only MYXV-treated individuals survived a total of 6 weeks (41 days) under observation. Calculations show the probability for each mouse to survive 41 days post tail vein injection. Mice tissues harvested during planned endpoints were analyzed for pathology. Early sacrifice was unforeseen and did not allow time for tissue collection.

+++ = animal showed no signs of engraftment in post mortem analysis

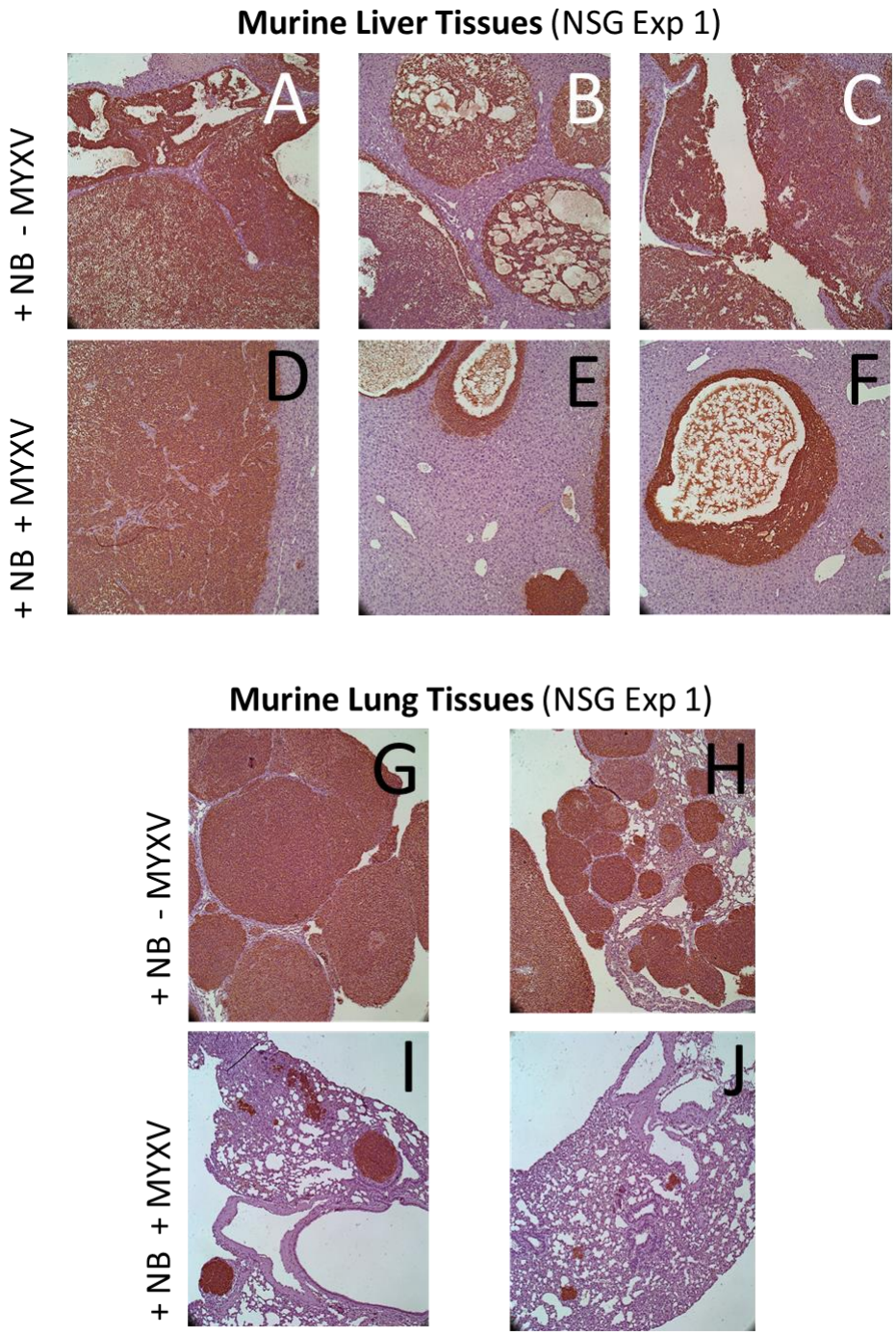

Figure 3-4. NSG Experiment 1: Reduced engraftment of SK-N-AS in MYXV-treated animals, following intravenous injection of 2.86×10^6 SK-N-AS in sub-lethally irradiated mice. The most aggressive examples of MYXV induced killing of SK-N-AS is seen within lung tissues. Tumor necrosis is visible in samples from murine liver tissues (B,E,F). Results show tissues collected from one animal in each cohort (Mock or MYXV). Corresponding liver and lung samples are from the same animal.

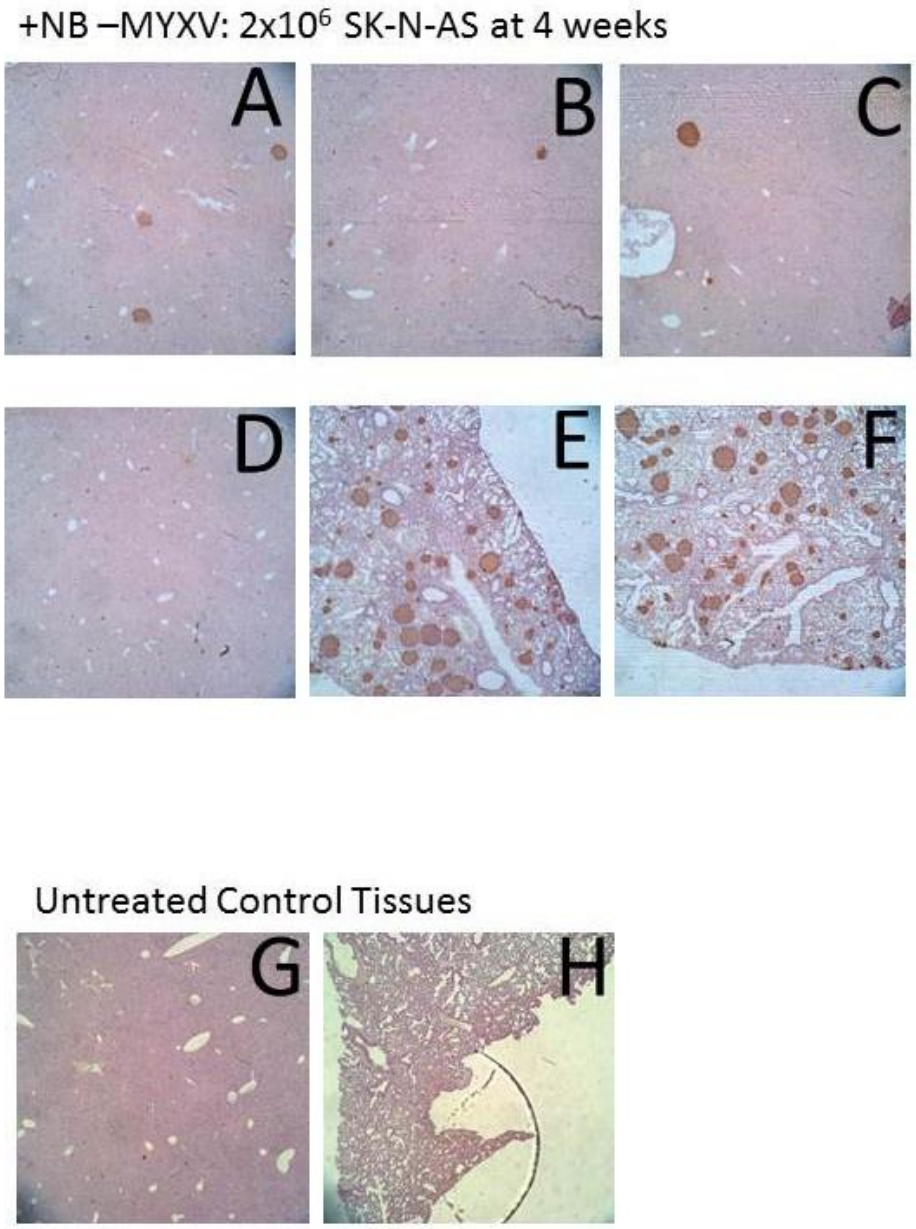

Figure 3-5. Preliminary Experiment: Overall SK-N-AS engraftment for Mock-treated animals. Images were taken at 20X magnification to allow visualization of larger area within histology section. Mice were not sub-lethally irradiated and tissues were harvested at 4 weeks post injection. Provided here are results for those animals which received $2x10^6$ cells that were not incubated with vMyx-eGFP. Both murine liver tissues (A-D, G) and lung tissues (E-F, H) are shown.

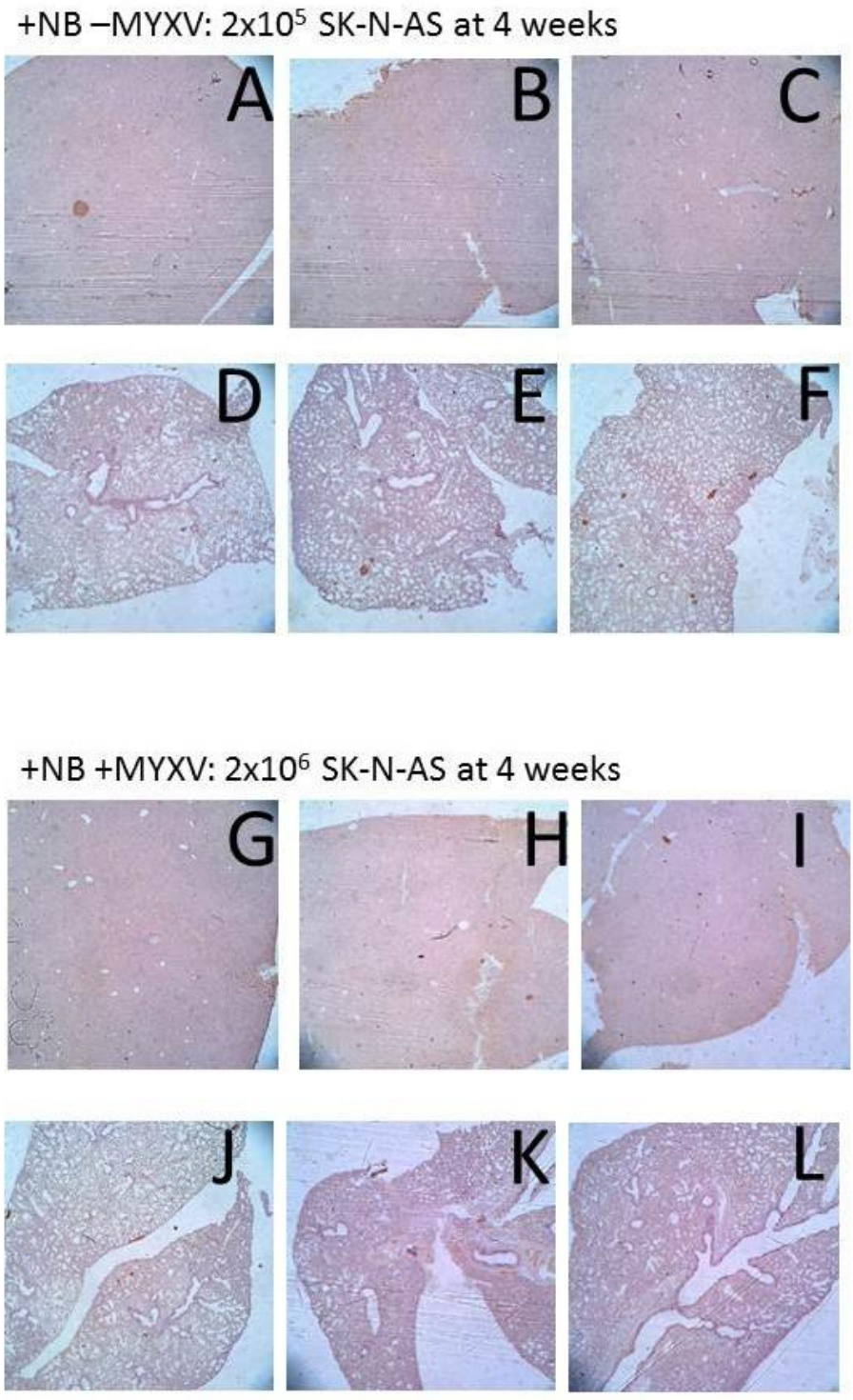

Figure 3-6. Preliminary Experiment: Overall SK-N-AS engraftment for MYXV-treated animals receiving $2x10^6$ cells. This shows reduced engraftment comparable to Mock animals that only received $2x10^5$ SK-N-AS. In non-irradiated NSG mice, MYXV treatment on adherent cells (MOI 25) reduces SK-N-AS engraftment comparable to1 log difference. Tissues were harvested at 4 weeks post injection and images taken at 20X magnification.

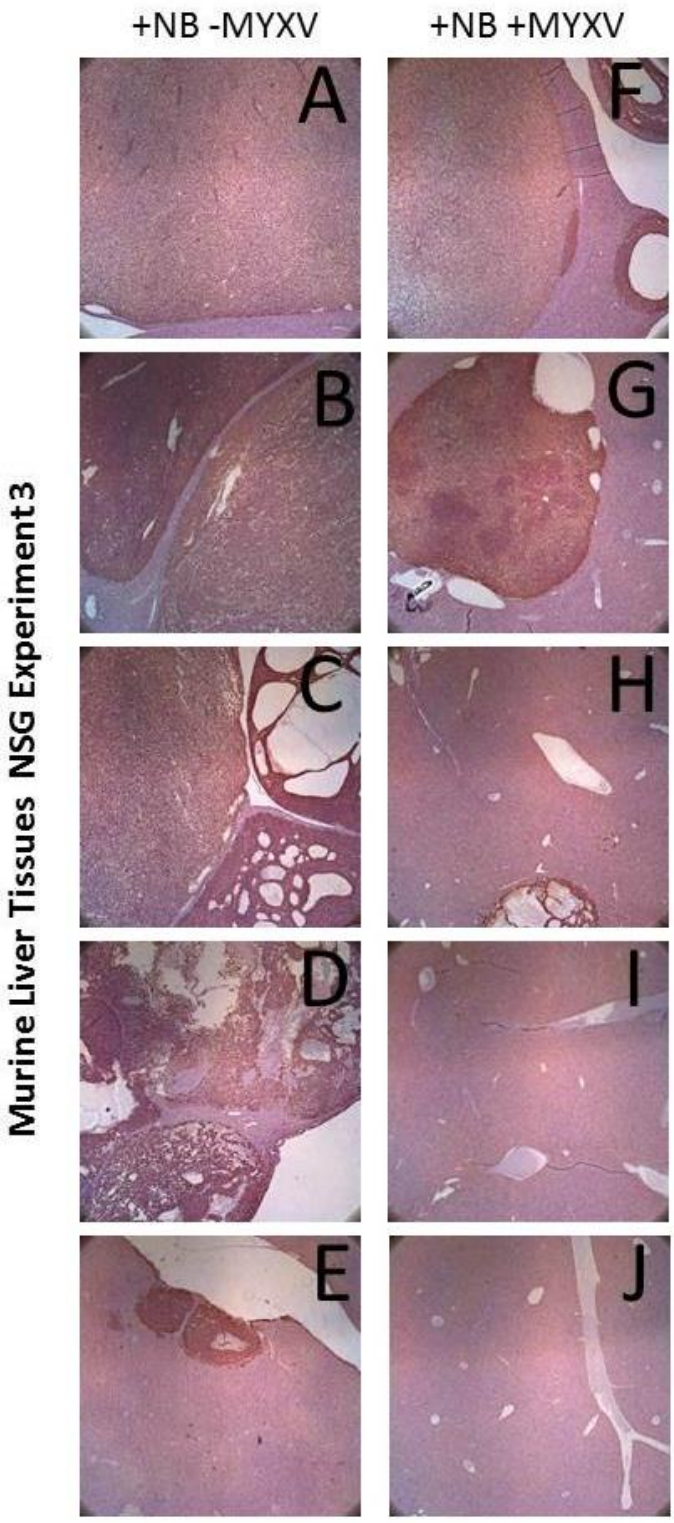

Figure 3-7. Histology of tumor cell engraftment in murine liver tissues (NSG Exp 3): each NSG received $2x10^5$ SK-N-AS pre-treated with vMyx-eGFP (MOI 10 or 0) on adherent cells. Mice were previously irradiated and tissues were harvested during the 6^{th} week after injection (day 45). Figures are arranged by decreasing levels of engraftment.

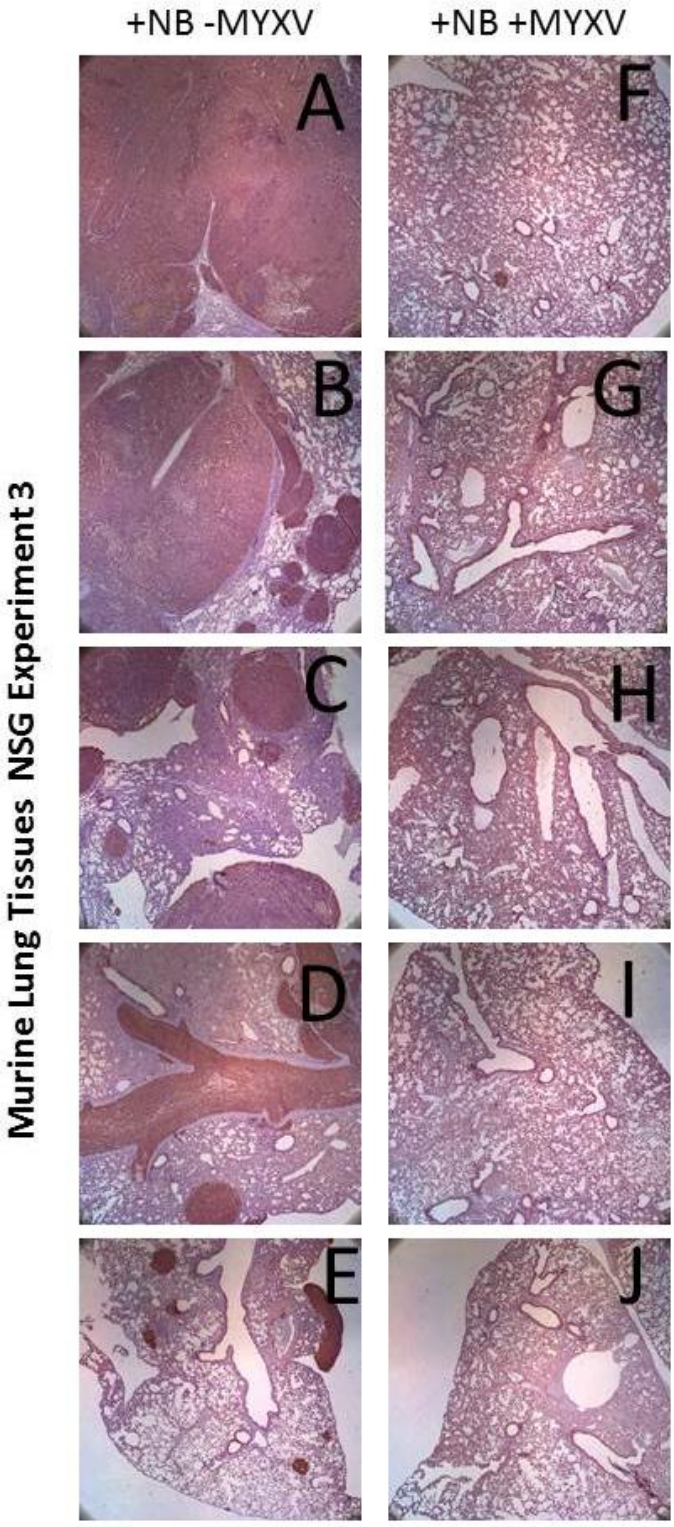

Figure 3-8. Histology of murine lung tissues (NSG Exp 3): each NSG received $2x10^5$ SK-N-AS pre-treated with vMyx-eGFP (MOI 10 or 0) on adherent cells. Mice were previously irradiated and tissues were harvested during the 6^{th} week after injection (day 45). Figures are arranged by decreasing levels of engraftment.

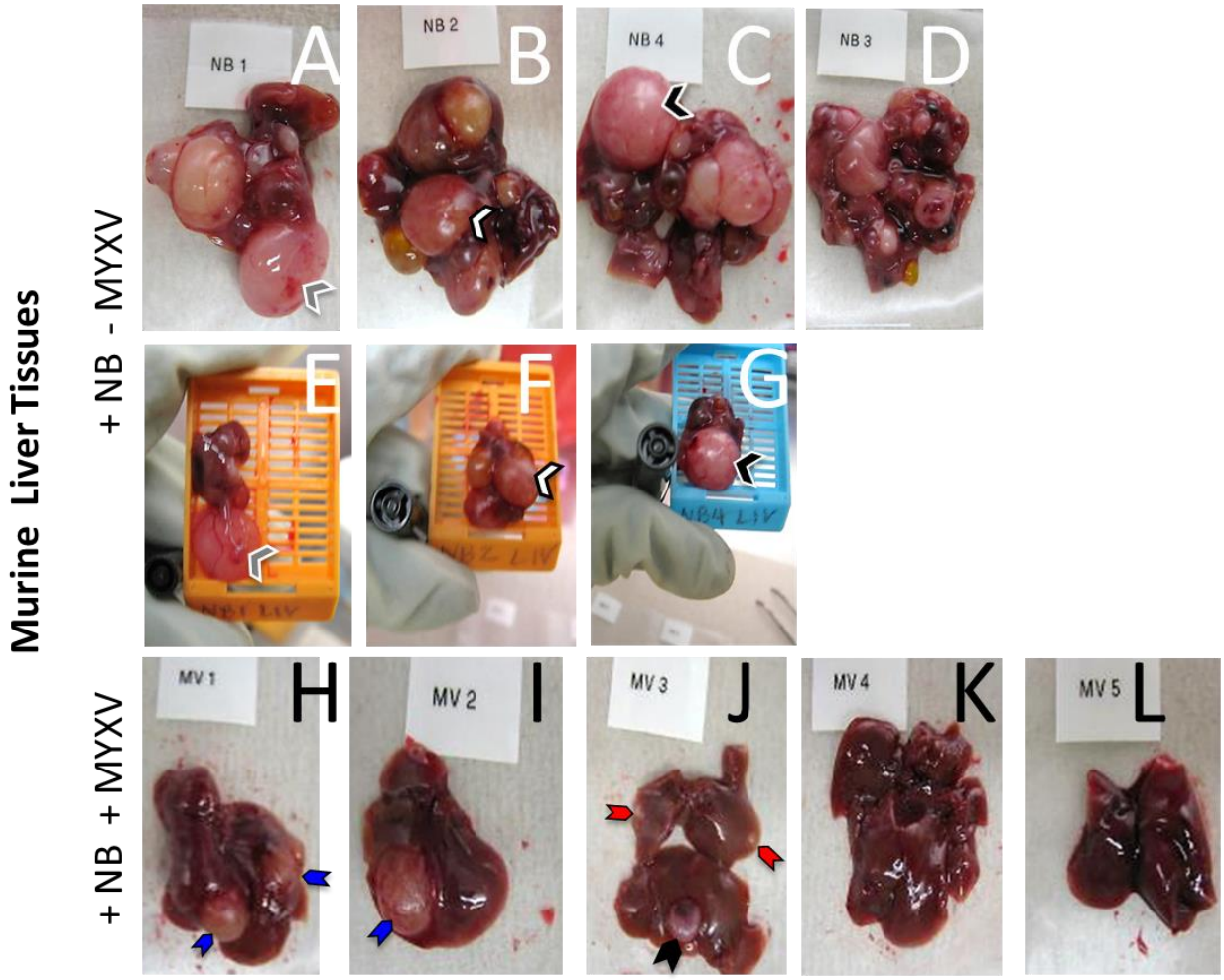

Figure 3-9. Necropsy observations for murine liver tissues (NSG EXP 3). Mice were sub-lethally irradiated and received $2x10^5$ SK-N-AS each. MYXV treatment: vMyx-eGFP on adherent cells, MOI 10. All animals showed enlarged tissues in cancer-affected organs. Sample labels (top, center, each figure) correspond with those in Table 3-5. Labels were all printed uniformly and can be used to gauge respective tissue size. Notice that NB3 and NB4 are not listed in chronological order. A-C) Images represent only one lobe of the liver. D) Complete resection of all liver tissues in NB3. E-G) The same liver tissues presented as above in A-C. Size is shown in comparison to the top of a pen cap (black, lower left corner). For images A-G) large arrowheads provide orientation to track the same tissues as visualized in different images. Matching colors indicate identical tissues. For images H-L) these small arrowhead colors do not indicate identical tissues. BLUE arrows =large growths. BLACK=medium. RED=small.

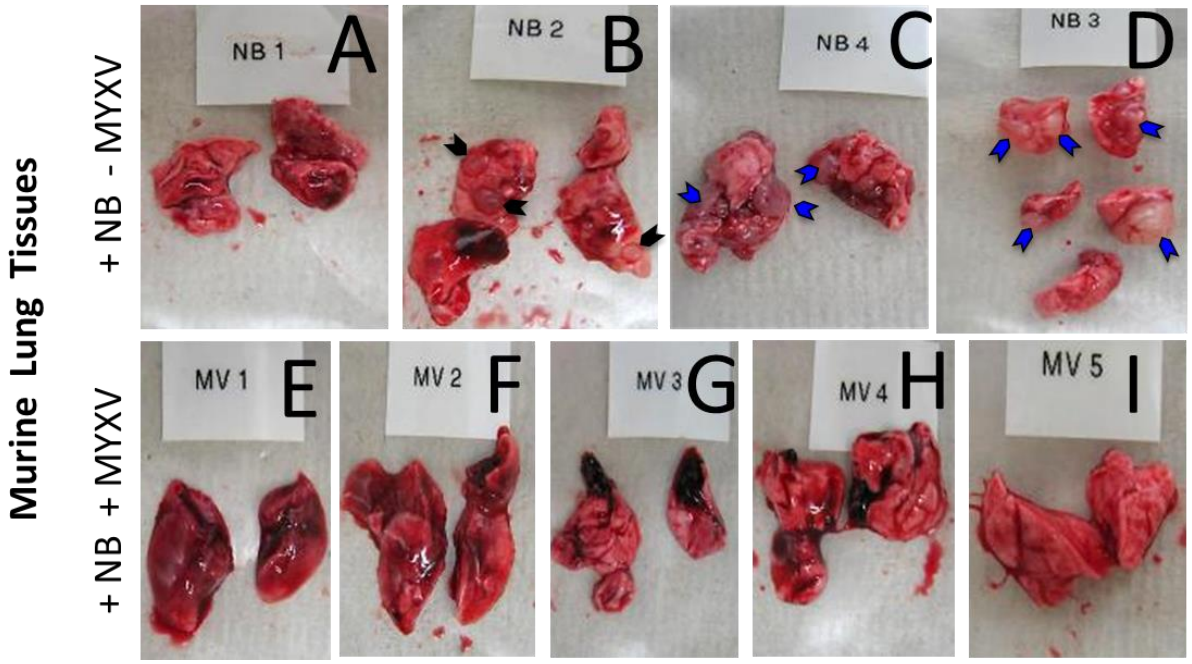

Figure 3-10. Necropsy observations for murine lung tissues (NSG EXP 3). Mice were sub-lethally irradiated and received $2x10^5$ SK-N-AS each. MYXV treatment: vMyx-eGFP on adherent cells, MOI 10. Sample labels (top, center, each figure) correspond with those in Table 3-5. Labels were all printed uniformly and can be used to gauge respective tissue size. Notice that NB3 and NB4 are not listed in chronological order. B-D) For small arrow heads, colors do not indicate identical tissues. Small arrowheads: BLUE arrows =large growths. BLACK=medium. RED=small. B) Medium sized growths are difficult to see because they have not yet formed into tumors that project off the surface of the organ.

CHAPTER 4
DISCUSSION

Interpretation of Results

Myxoma Virus (MYXV) is able to infect and kill cultured human SK-N-AS neuroblastoma cells. In previous work using MYXV as an oncolytic agent against other types of human cancer cells, virus-induced cell killing of multiple myeloma cells only required the attachment of virions to cancer cell surfaces[1]. The present study showed that MYXV is able to infect and grow exponentially in SK-N-AS cells, thereby releasing new progeny virions that can infect and result in the death of more cells in the same culture. This depletes the neuroblastoma cell population at a greater level than what the amount of input virus would exhibit in the absence of virus amplification. Also, virus adsorption conditions were found to affect the level of virus infection, and thus MYXV-adsorption in future experiments should be performed on cancer cells suspended in the liquid inoculum at an increased ratio of cells per total volume. This suspension adsorption could potentially also improve the likelihood for newly released virions to bind and enter any remaining cancer cells that were not infected during previous replication cycles. We expect that the number of chance interactions arising between cells will also increase by bringing cells into close proximity with each other. This would be the preferred *ex vivo* strategy for MYXV treatment of bone marrow samples from neuroblastoma patients; to decontaminate all potentially contaminating cancer cells in the transplant sample prior to engraftment.

When SK-N-AS cells were treated *ex vivo* by MYXV, cell death ensued and this visibly reduced the level of SK-N-AS engraftment into transplant recipient NSG mice. This decrease in tumor establishment in recipient mice was demonstrated *in vivo*

through the lessening of disease phenotypes in both murine tissue anatomy and in terms of reduced clinical symptoms. MYXV-treatment consistently resulted in these tumor reduction effects, in spite of the suboptimal conditions that were used for the virus adsorption conditions prior to transplant. Therefore, by targeting improved parameters for MYXV-treatment, we foresee a further increase in MYXV efficiency at reducing subsequent tumor burden.

There was only one *in vivo* experiment that utilized the now-preferred method of pre-MYXV adsorption with liquid-suspended cells (i.e. NSG Exp 1). In this and all other xenotransplants, MYXV was shown to substantially reduce, but not fully protect, NSG mice from SK-N-AS engraftment. According to *Poisson's distribution*, we would expect that 99.95% of all cells received >1 FFU at the MOI of 10, if all cells are equally available to the input virus. However, virus-induced cell death was not achieved at this same rate, and was considerably less than the near-universal cell killing observed in similar MYXV treatment of human multiple myeloma cells[1]. NSG 1 treatment groups received the highest dosage of SK-N-AS cells in the initial graft sample. It was considered that even if only 0.05% of the total cell population encounters $\leq$1 FFU per cell, this may have been enough to establish subsequent engraftment. However in the cell dose de-escalation study, $2x10^3$ input SK-N-AS cells cannot induce detectable engraftment of tumors within 6 weeks post injection; this is shown in non-irradiated mice, but a similar dose-down cohort was not tested for the more tumor-prone sub-lethally irradiated animals.

If SK-N-AS cells require a higher FFU per cell ratio to induce uniform levels of cell death, this explains our inability to completely protect animals by pre-treatment of

cancer cells with MYXV. Future studies could establish the minimum MOI required for successful MYXV pretreatment of *bona fide* neuroblastoma bone marrow transplant specimens, which may contain low, but often undefined, levels of cancer cell contamination. From the alternative perspective, it would be beneficial to determine the maximum number of cells (per injection regimen in an individual NSG mouse) that can be killed with high efficiency by *ex vivo* pretreatment with MYXV. For a genuine clinical application, MYXV purging of cancer cells from a stem cell transplant specimen (either bone marrow or mobilized PBMCs) would be incorporated as one component of a multimodal treatment plan. Since MYXV purging would either follow or be used in combination with other standard therapies, there is the possibility that MYXV will be used to treat overall lower numbers of contaminating cells per autograft sample. In patients containing high residual disease, one could also take advantage of the ability to further manipulate the *ex vivo* MYXV infection conditions, by the viral adsorption of patient samples in the optimum inoculum volume for MYXV treatment. Afterwards, individual treatment aliquots could be recombined for return to the patient via autologous transplantation.

There may also be a minimum threshold of MYXV replication that is required for the optimal killing of SK-N-AS cells. Massive cell death *in vitro* is not detected until the third day following initial infection, and the continued expansion of some GFP-positive colonies shows that residual levels of cells can survive in culture when minimally infected with low amounts of replicating virus. Initial rounds of MYXV replication in SK-N-AS are relatively slow compared to control cells like BSC-40 cells, maximal viral yields peak more than 24 hours post-infection, and MYXV-induced killing is observed

(though not as efficiently as in multiple myeloma cells, for example). There is a need to uncover a strategy to decrease the lag time between initial infection and the killing of neuroblastoma cells. In speculation, it is possible that cell death is induced by the accumulation of certain viral products expressed within the infected cells. Future experiments may attempt to more accurately track temporal viral protein synthesis in comparison to cell death kinetics over time. If a specific viral "cell death" factor were identified, one could potentially design a recombinant virus that overexpresses that gene during the MYXV replication cycle.

This thesis has tested a novel xenograft transplant model for MYXV therapy of neuroblastoma. Due to the benefit of increased sensitivity to the appearance of developing tumors, all future studies should be conducted in sub-lethally irradiated mice, which better represents immunocompromised neuroblastoma patients who receive stem cell autotransplants. The six-week time point post-infusion allows for the sufficient development of different disease phenotypes within treatment groups (when $2x10^5$ SK-N-AS cells are transplanted per mouse). Related xenograft models of neuroblastoma currently being investigated include the SK-N-AS cell line in Nu/Nu nude and SCID mice, or other neuroblastoma cell lines in NSG mice. For routes of administration, subcutaneous is the most commonly exploited method[36, 37, 38]. Unlike a previous description of NSG xenotransplantation, we did not observe disease metastasis to organs that reflect human recurrent neuroblastoma disease[38]. Our purging model employs observations of engraftment to gauge MYXV efficiency at the reduction of disease-inducing cells from potential autologous graft samples. For this reason, the actual site of subsequent tumor development was of less concern. Our work is the first

account of SK-N-AS engraftment in NSG mice and now adds to the growing list of cell lines that could provide insights into tumor formation in these animals. A diversity of tumor growth phenotypes was observed in recipient mice and we expect that this will be even more relevant during the testing of actual primary patient autografts in future work.

Consideration of Unexpected Results

The two cell viability assays tested in this thesis gave different results. When infected with virus at optimum conditions, MYXV-infected cells cannot form colonies in culture. Suspension-treated SK-N-AS cells in this non-adherent state, do not survive 97% of the time. In contrast, MYXV reduces cell viability by the lesser value of 80% when the virus is adsorbed onto adherent SK-N-AS cells. This may be a reflection of the nonequivalent binding efficiency of virus particles between the two different methods of infection. Moreover, a true comparison would require the observation of cells in both treatment groups for an equal length of time. There are also other possible explanations. For example, MYXV killing may only occur at 80% efficiency within both treatment groups. Instead, suspension-infected cells may lose the ability to re-attach to culture dishes, resulting in the eventual diminishment of survival down to 3%. If we are able to induce SK-N-AS to grow in suspension, we could then test to see if MYXV-induced death is related to anchorage dependence (for example, in a CFU assay in which cells are suspended in an agar overlay). The consideration of SK-N-AS requirements for surface adhesion could be significant, because any contaminating neuroblastoma that is present in patient stem cell autografts probably results from cancer cell metastasis to the bone marrow or as free cells in the circulation. This means that our target cell population for purging could exhibit unique virus-binding characteristics. Metastatic cells are associated with loss of anchorage dependence,

detachment from the primary tumor, migration, and then re-gain of the ability to adhere to and invade tissues[39].

It was observed that sub-lethally irradiated NSG mice are more susceptible to SK-N-AS engraftment and levels of subsequent disease burden. This may occur for many reasons. One possibility is the existence of a subpopulation of MYXV-resistant cells within the SK-N-AS cell cultures used in the study. These cells may be more aggressive in growth and could also be the only cells able to persist in non-irradiated mice. However, our investigation of GFP-expressing colonies does not seem to support the existence of a virus-resistant subpopulation of SK-N-AS cells. In another scenario, there may be a burden over which the minimal host responses that are available in NSG mice (myeloid cells for example) succumb to critical threshold levels of tumor development. Those SK-N-AS cells that engraft into NSG mice may benefit from the fact that these limited innate immune defenses have become overwhelmed. This question could be addressed by extending the length of time for tumor growth in non-irradiated mice, followed by an investigation of the seeded tumors.

Strengths and Weaknesses

Weaknesses of this study include the need for increased repetition and larger animal cohort sizes to establish statistical significance of the MYXV effects on subsequent tumor development. The main concern was the lack of a method for quantification of *in vivo* results in terms of precise tumor burdens. In the preferred outcome, we would have used a stable luciferase-expressing SK-N-AS cell line for the *in vivo* visualization and quantification of tumors. During the course of this project, I began the construction of an SK-N-AS derived cell line that expressed Firefly luciferase activity. However, there was not enough time to: generate a homogenous sub-clonal

population with stable luciferase expression; to characterize the cell line *in vitro;* or to use in the animal cohorts. In the absence of luciferase-expressing SK-N-AS, we relied on qualitative methods of tissue analysis for untagged SK-N-AS tumors. For this reason, the interpretation of results is limited in terms of quantification of the exact reductions in tumor burden caused by the MYXV treatments. Future work involving a luciferase-expressing cell line will improve the established xenograft model and make it easier to establish statistically significant differences between treatment groups. One benefit is that all tissue sections from the studies reported in this thesis have been formalin preserved and embedded in paraffin, providing a means for review at a later time.

It would also be beneficial to include additional neuroblastoma cell lines in future studies. SK-N-AS originates from metastasis in the bone marrow and exhibits the characteristic deletion of chromosome 1p, an indicator of high-risk disease[40]. Other cell lines to include should represent the wider diversity of neuroblastoma phenotypes, such as amplification of the MYCN oncogene. In hindsight, the benefit of working with one cell line was that we were able to establish a standard of tumor development expectations in the xenograft model in irradiated NSG mice. This made it easier to identify deviations that may otherwise have been overlooked.

Future Work and Implications

The potential of MYXV therapy for treating autologous neuroblastoma stem cell transplant samples has been demonstrated both in vitro and in vivo. MYXV is able to infect and replicate within the human cell line SK-N-AS, resulting ultimately in cell death. Future work should include a comparison against other cancer cell purging methods (positive CD34+ cell selection, monoclonal antibodies, immunomagnetic cell separation strategies, conjugated toxin, and chemotherapy). Inconsistencies in the reliability and

benefit of these procedures have been described elsewhere[41, 42, and 43]. We believe that MYXV specificity and efficiency may be an improvement over current cancer cell purging standards. Another goal is to study MYXV ability to purge actual neuroblastoma patient autografts in the same *ex vivo* treatment model described here, as we have reported elsewhere for primary human multiple myeloma bone marrow samples[1].

In the future development of MYXV as an oncolytic treatment, we will likely benefit from insights gained in the development of the closely related poxvirus, Vaccinia Virus. The vaccinia strain JX-929[44] is genetically modified for tissue tropism and currently undergoing clinical investigations for a number of solid tumors, including liver cancer[45]. At the present time, conflicting reports have aroused disagreement among clinicians over the benefits (or lack thereof) for cancer cell purging of autografts for neuroblastoma. However, the disputed experiments did not allow for direct comparison between purged and non-purged samples, or were confined by the limitations of a retrospective analysis[46, 47]. Therefore, it is the author's opinion that these prior studies neither dispel nor support purging as a strategy to improve the survival of neuroblastoma patients who receive autologous stem cell transplants.

Overall, this study supports the continued investigation of MYXV therapy as an *ex vivo* purging agent for neuroblastoma patients. We hope to aid in the discovery of new therapeutic options that will result in higher rates of relapse-free long term patient survival and an improvement in the quality of life for children suffering from the most high-risk form of this disease.

LIST OF REFERENCES

1. **Bartee, E., W. M. Chan, J. S. Moreb, C. R. Cogle, and G. McFadden.** 2012. Selective purging of human multiple myeloma cells from autologous stem cell transplantation grafts using oncolytic myxoma virus. Biol. Blood Marrow Transplant. **18:**1540-1551. doi: 10.1016/j.bbmt.2012.04.004; 10.1016/j.bbmt.2012.04.004.

2. **Wennier, S. T., J. Liu, S. Li, M. M. Rahman, M. Mona, and G. McFadden.** 2012. Myxoma virus sensitizes cancer cells to gemcitabine and is an effective oncolytic virotherapeutic in models of disseminated pancreatic cancer. Mol. Ther. **20:**759-768. doi: 10.1038/mt.2011.293; 10.1038/mt.2011.293.

3. **Madlambayan, G. J., E. Bartee, M. Kim, M. M. Rahman, A. Meacham, E. W. Scott, G. McFadden, and C. R. Cogle.** 2012. Acute myeloid leukemia targeting by myxoma virus in vivo depends on cell binding but not permissiveness to infection in vitro. Leuk. Res. **36:**619-624. doi: 10.1016/j.leukres.2012.01.020; 10.1016/j.leukres.2012.01.020.

4. **Kerr, P. J.** 2012. Myxomatosis in Australia and Europe: a model for emerging infectious diseases. Antiviral Res. **93:**387-415. doi: 10.1016/j.antiviral.2012.01.009; 10.1016/j.antiviral.2012.01.009.

5. **McFadden, G.** 2005. Poxvirus tropism. Nat. Rev. Microbiol. **3:**201-213. doi: 10.1038/nrmicro1099.

6. **Sypula, J., F. Wang, Y. Ma, J. Bell, and G. McFadden.** April 20, 2004. **Myxoma virus tropism in human tumor cells**. Gene Ther Mol Biol. **March 1, 2013:**103-114.

7. **Bartee, E., and G. McFadden.** 2009. Human cancer cells have specifically lost the ability to induce the synergistic state caused by tumor necrosis factor plus interferon-beta. Cytokine. **47:**199-205. doi: 10.1016/j.cyto.2009.06.006; 10.1016/j.cyto.2009.06.006.

8. **Bartee, E., M. R. Mohamed, M. C. Lopez, H. V. Baker, and G. McFadden.** 2009. The addition of tumor necrosis factor plus beta interferon induces a novel synergistic antiviral state against poxviruses in primary human fibroblasts. J. Virol. **83:**498-511. doi: 10.1128/JVI.01376-08; 10.1128/JVI.01376-08.

9. **Chan, W. M., E. C. Bartee, J. S. Moreb, K. Dower, J. H. Connor, and G. McFadden.** 2013. Myxoma and vaccinia viruses bind differentially to human leukocytes. J. Virol. **87:**4445-4460. doi: 10.1128/JVI.03488-12; 10.1128/JVI.03488-12.

10. **Kim, M., G. J. Madlambayan, M. M. Rahman, S. E. Smallwood, A. M. Meacham, K. Hosaka, E. W. Scott, C. R. Cogle, and G. McFadden.** 2009. Myxoma virus targets primary human leukemic stem and progenitor cells while

sparing normal hematopoietic stem and progenitor cells. Leukemia. **23:**2313-2317. doi: 10.1038/leu.2009.219; 10.1038/leu.2009.219.

11. **Chan, W. M., M. M. Rahman, and G. McFadden.** 2013. Oncolytic myxoma virus: The path to clinic. Vaccine. doi: 10.1016/j.vaccine.2013.05.056; 10.1016/j.vaccine.2013.05.056.

12. **Bourke, M. G., S. Salwa, K. J. Harrington, M. J. Kucharczyk, P. F. Forde, M. de Kruijf, D. Soden, M. Tangney, J. K. Collins, and G. C. O'Sullivan.** 2011. The emerging role of viruses in the treatment of solid tumours. Cancer Treat. Rev. **37:**618-632. doi: 10.1016/j.ctrv.2010.12.003; 10.1016/j.ctrv.2010.12.003.

13. **Smith, M. A., N. L. Seibel, S. F. Altekruse, L. A. Ries, D. L. Melbert, M. O'Leary, F. O. Smith, and G. H. Reaman.** 2010. Outcomes for children and adolescents with cancer: challenges for the twenty-first century. J. Clin. Oncol. **28:**2625-2634. doi: 10.1200/JCO.2009.27.0421; 10.1200/JCO.2009.27.0421.

14. **Stiller, C. A., and D. M. Parkin.** 1992. International variations in the incidence of neuroblastoma. Int. J. Cancer. **52:**538-543.

15. **Park, J. R., A. Eggert, and H. Caron.** 2010. Neuroblastoma: biology, prognosis, and treatment. Hematol. Oncol. Clin. North Am. **24:**65-86. doi: 10.1016/j.hoc.2009.11.011; 10.1016/j.hoc.2009.11.011.

16. **Pugh, T. J., O. Morozova, E. F. Attiyeh, S. Asgharzadeh, J. S. Wei, D. Auclair, S. L. Carter, K. Cibulskis, M. Hanna, A. Kiezun, J. Kim, M. S. Lawrence, L. Lichenstein, A. McKenna, C. S. Pedamallu, A. H. Ramos, E. Shefler, A. Sivachenko, C. Sougnez, C. Stewart, A. Ally, I. Birol, R. Chiu, R. D. Corbett, M. Hirst, S. D. Jackman, B. Kamoh, A. H. Khodabakshi, M. Krzywinski, A. Lo, R. A. Moore, K. L. Mungall, J. Qian, A. Tam, N. Thiessen, Y. Zhao, K. A. Cole, M. Diamond, S. J. Diskin, Y. P. Mosse, A. C. Wood, L. Ji, R. Sposto, T. Badgett, W. B. London, Y. Moyer, J. M. Gastier-Foster, M. A. Smith, J. M. Auvil, D. S. Gerhard, M. D. Hogarty, S. J. Jones, E. S. Lander, S. B. Gabriel, G. Getz, R. C. Seeger, J. Khan, M. A. Marra, M. Meyerson, and J. M. Maris.** 2013. The genetic landscape of high-risk neuroblastoma. Nat. Genet. **45:**279-284. doi: 10.1038/ng.2529; 10.1038/ng.2529.

17. **Mosse, Y. P., M. Laudenslager, L. Longo, K. A. Cole, A. Wood, E. F. Attiyeh, M. J. Laquaglia, R. Sennett, J. E. Lynch, P. Perri, G. Laureys, F. Speleman, C. Kim, C. Hou, H. Hakonarson, A. Torkamani, N. J. Schork, G. M. Brodeur, G. P. Tonini, E. Rappaport, M. Devoto, and J. M. Maris.** 2008. Identification of ALK as a major familial neuroblastoma predisposition gene. Nature. **455:**930-935. doi: 10.1038/nature07261; 10.1038/nature07261.

18. **Mosse, Y. P., M. Laudenslager, D. Khazi, A. J. Carlisle, C. L. Winter, E. Rappaport, and J. M. Maris.** 2004. Germline PHOX2B mutation in hereditary neuroblastoma. Am. J. Hum. Genet. **75:**727-730. doi: 10.1086/424530.

19. **Trochet, D., F. Bourdeaut, I. Janoueix-Lerosey, A. Deville, L. de Pontual, G. Schleiermacher, C. Coze, N. Philip, T. Frebourg, A. Munnich, S. Lyonnet, O. Delattre, and J. Amiel.** 2004. Germline mutations of the paired-like homeobox 2B (PHOX2B) gene in neuroblastoma. Am. J. Hum. Genet. **74:**761-764. doi: 10.1086/383253.

20. **London, W. B., R. P. Castleberry, K. K. Matthay, A. T. Look, R. C. Seeger, H. Shimada, P. Thorner, G. Brodeur, J. M. Maris, C. P. Reynolds, and S. L. Cohn.** 2005. Evidence for an age cutoff greater than 365 days for neuroblastoma risk group stratification in the Children's Oncology Group. J. Clin. Oncol. **23:**6459-6465. doi: 10.1200/JCO.2005.05.571.

21. **McConville, C. M., and J. Forsyth.** 2003. Neuroblastoma - a developmental perspective. Cancer Lett. **197:**3-9.

22. **Jiang, M., J. Stanke, and J. M. Lahti.** 2011. The connections between neural crest development and neuroblastoma. Curr. Top. Dev. Biol. **94:**77-127. doi: 10.1016/B978-0-12-380916-2.00004-8; 10.1016/B978-0-12-380916-2.00004-8.

23. **Marusich, M. F., and J. A. Weston.** 1991. Development of the neural crest. Curr. Opin. Genet. Dev. **1:**221-229.

24. **Francis, N. J., and S. C. Landis.** 1999. Cellular and molecular determinants of sympathetic neuron development. Annu. Rev. Neurosci. **22:**541-566. doi: 10.1146/annurev.neuro.22.1.541.

25. **Brodeur, G. M., J. Pritchard, F. Berthold, N. L. Carlsen, V. Castel, R. P. Castelberry, B. De Bernardi, A. E. Evans, M. Favrot, and F. Hedborg.** 1993. Revisions of the international criteria for neuroblastoma diagnosis, staging, and response to treatment. J. Clin. Oncol. **11:**1466-1477.

26. **Maris, J. M.** 2010. Recent advances in neuroblastoma. N. Engl. J. Med. **362:**2202-2211. doi: 10.1056/NEJMra0804577; 10.1056/NEJMra0804577.

27. **Modak, S., and N. K. Cheung.** 2010. Neuroblastoma: Therapeutic strategies for a clinical enigma. Cancer Treat. Rev. **36:**307-317. doi: 10.1016/j.ctrv.2010.02.006; 10.1016/j.ctrv.2010.02.006.

28. **Matthay, K. K., J. G. Villablanca, R. C. Seeger, D. O. Stram, R. E. Harris, N. K. Ramsay, P. Swift, H. Shimada, C. T. Black, G. M. Brodeur, R. B. Gerbing, and C. P. Reynolds.** 1999. Treatment of high-risk neuroblastoma with intensive chemotherapy, radiotherapy, autologous bone marrow transplantation, and 13-cis-retinoic acid. Children's Cancer Group. N. Engl. J. Med. **341:**1165-1173. doi: 10.1056/NEJM199910143411601.

29. **Berthold, F., J. Boos, S. Burdach, R. Erttmann, G. Henze, J. Hermann, T. Klingebiel, B. Kremens, F. H. Schilling, M. Schrappe, T. Simon, and B. Hero.** 2005. Myeloablative megatherapy with autologous stem-cell rescue versus oral

maintenance chemotherapy as consolidation treatment in patients with high-risk neuroblastoma: a randomised controlled trial. Lancet Oncol. **6:**649-658. doi: 10.1016/S1470-2045(05)70291-6.

30. **Rill, D. R., V. M. Santana, W. M. Roberts, T. Nilson, L. C. Bowman, R. A. Krance, H. E. Heslop, R. C. Moen, J. N. Ihle, and M. K. Brenner.** 1994. Direct demonstration that autologous bone marrow transplantation for solid tumors can return a multiplicity of tumorigenic cells. Blood. **84:**380-383.

31. **Kanold, J., K. Yakouben, A. Tchirkov, A. S. Carret, J. P. Vannier, E. LeGall, P. Bordigoni, and F. Demeocq.** 2000. Long-term results of CD34(+) cell transplantation in children with neuroblastoma. Med. Pediatr. Oncol. **35:**1-7.

32. **Marabelle, A., E. Merlin, P. Halle, C. Paillard, M. Berger, A. Tchirkov, R. Rousseau, G. Leverger, C. Piguet, J. L. Stephan, F. Demeocq, and J. Kanold.** 2011. CD34+ immunoselection of autologous grafts for the treatment of high-risk neuroblastoma. Pediatr. Blood Cancer. **56:**134-142. doi: 10.1002/pbc.22840; 10.1002/pbc.22840.

33. **Johnston, J. B., J. W. Barrett, W. Chang, C. S. Chung, W. Zeng, J. Masters, M. Mann, F. Wang, J. Cao, and G. McFadden.** 2003. Role of the serine-threonine kinase PAK-1 in myxoma virus replication. J. Virol. **77:**5877-5888.

34. **Smallwood, S. E., M. M. Rahman, D. W. Smith, and G. McFadden.** 2010. Myxoma virus: propagation, purification, quantification, and storage. Curr. Protoc. Microbiol. **Chapter 14:**Unit 14A.1. doi: 10.1002/9780471729259.mc14a01s17; 10.1002/9780471729259.mc14a01s17.

35. **Ullman-Cullere, M. H., and C. J. Foltz.** 1999. Body condition scoring: a rapid and accurate method for assessing health status in mice. Lab. Anim. Sci. **49:**319-323.

36. **Meco, D., A. M. Di Francesco, G. Cusano, F. Bucci, F. Pierri, V. Patriarca, A. R. Torella, C. Pisano, and R. Riccardi.** 2012. Preclinical evaluation of the novel 7-substituted camptothecin Namitecan (ST1968) in paediatric tumour models. Cancer Chemother. Pharmacol. **70:**811-822. doi: 10.1007/s00280-012-1973-0; 10.1007/s00280-012-1973-0.

37. **Rouleau, C., K. Menon, P. Boutin, C. Guyre, H. Yoshida, S. Kataoka, M. Perricone, S. Shankara, A. E. Frankel, N. S. Duesbery, G. Vande Woude, H. P. Biemann, and B. A. Teicher.** 2008. The systemic administration of lethal toxin achieves a growth delay of human melanoma and neuroblastoma xenografts: assessment of receptor contribution. Int. J. Oncol. **32:**739-748.

38. **Sartelet, H., L. Durrieu, F. Fontaine, C. Nyalendo, and E. Haddad.** 2012. Description of a new xenograft model of metastatic neuroblastoma using NOD/SCID/Il2rg null (NSG) mice. In Vivo. **26:**19-29.

39. **Ara, T., and Y. A. DeClerck.** 2006. Mechanisms of invasion and metastasis in human neuroblastoma. Cancer Metastasis Rev. **25:**645-657. doi: 10.1007/s10555-006-9028-9.

40. **Thiele, C. J.** 1998. Neuroblastoma Cell Lines, p. 21-53. *In* J. Masters (ed.), Human Cell Culturevol. 1. Kluwer Academic Publishers, Lancaster, UK.

41. **Lopez, M., and F. Beaujean.** 1999. Positive selection of autologous peripheral blood stem cells. Baillieres Best Pract. Res. Clin. Haematol. **12:**71-86.

42. **Shimoni, A., and M. Korbling.** 2002. Tumor cell contamination in re-infused stem cell autografts: does it have clinical significance? Crit. Rev. Oncol. Hematol. **41:**241-250.

43. **Voigt, A., R. Hafer, B. Gruhn, and F. Zintl.** 1997. Expression of CD34 and other haematopoietic antigens on neuroblastoma cells: consequences for autologous bone marrow and peripheral blood stem cell transplantation. J. Neuroimmunol. **78:**117-126.

44. http://www.jennerex.com/patient-resources.html

45. **Heo, J., T. Reid, L. Ruo, C. J. Breitbach, S. Rose, M. Bloomston, M. Cho, H. Y. Lim, H. C. Chung, C. W. Kim, J. Burke, R. Lencioni, T. Hickman, A. Moon, Y. S. Lee, M. K. Kim, M. Daneshmand, K. Dubois, L. Longpre, M. Ngo, C. Rooney, J. C. Bell, B. G. Rhee, R. Patt, T. H. Hwang, and D. H. Kirn.** 2013. Randomized dose-finding clinical trial of oncolytic immunotherapeutic vaccinia JX-594 in liver cancer. Nat. Med. **19:**329-336. doi: 10.1038/nm.3089; 10.1038/nm.3089.

46. **Corrias, M. V., R. Haupt, B. Carlini, S. Parodi, L. Rivabella, A. Garaventa, V. Pistoia, and S. Dallorso.** 2006. Peripheral blood stem cell tumor cell contamination and survival of neuroblastoma patients. Clin. Cancer Res. **12:**5680-5685. doi: 10.1158/1078-0432.CCR-06-0740.

47. **Park, J. R., J. G. Villablanca, W. B. London, R. B. Gerbing, D. Haas-Kogan, E. S. Adkins, E. F. Attiyeh, J. M. Maris, R. C. Seeger, C. P. Reynolds, K. K. Matthay** and Children's Oncology Group. 2009. Outcome of high-risk stage 3 neuroblastoma with myeloablative therapy and 13-cis-retinoic acid: a report from the Children's Oncology Group. Pediatr. Blood Cancer. 52:44-50. doi: 10.1002/pbc.21784; 10.1002/pbc.21784.

BIOGRAPHICAL SKETCH

Nikéa Chanel Aytes was born in Cherry Point, NC, eventually relocating to the central Florida area with her family. In 2006, she graduated from the International Baccalaureate Program at Seminole High School in Sanford, FL. As an undergraduate at the University of Florida, Nikéa pursued leadership roles dedicated to mentoring underrepresented and first-generation-college students like her self. She also developed interests in molecular biology, and was invited to join the Emerging Diseases/Arbovirus Research and Test laboratory at the UF College of Veterinary Medicine. Nikéa received her Bachelor of Science in animal biology during the fall of 2010. Upon graduation, she continued her work as a laboratory technician and was also selected as a post-baccalaureate scholar within UF's Emerging Pathogens Institute. In August 2011, Nikéa entered the UF program in Translational Biotechnology as an NSF research fellow. While matriculating this interdisciplinary program that bridged both scientific and business principles, Nikéa joined the laboratory of Grant McFadden. Here, she dedicated two years to the investigation of Myxoma Virus as an oncolytic tool for cancer therapy. In the summer of 2013, Nikéa served as an R&D intern for the start-up company, Veterinary Oncology Services, in Tampa, FL. This allowed her to pursue her passion for animal health, while also continuing to delve into cancer research. Going forward, Nikéa will continue her professional training within UF's biomedical science doctoral study program. She intends to dedicate her career to science education, while aiding in the development of new treatments to improve human and animal health.